Air pollution impacts due to petroleum extraction in the Norwegian Sea during the ACCESS aircraft campaign

Paolo Tuccella, Jennie L. Thomas, Kathy S. Law, Jean-Christophe Raut, Louis Marelle, Anke Roiger, B. Weinzierl, H. Denier van Der Gon, H. Schlager, Tatsuo Onishi

ELEMENTA
Science of the Anthropocene

Tuccella, P, et al 2017 Air pollution impacts due to petroleum extraction in the Norwegian Sea during the ACCESS aircraft campaign. *Elem Sci Anth,* 5: 25, DOI: https://doi.org/10.1525/elementa.124

RESEARCH ARTICLE

Air pollution impacts due to petroleum extraction in the Norwegian Sea during the ACCESS aircraft campaign

P. Tuccella[*,‖,¶], J. L. Thomas[*], K. S. Law[*], J.-C. Raut[*], L. Marelle[*,**], A. Roiger[†], B. Weinzierl[‡], H. A. C. Denier van der Gon[§], H. Schlager[†] and T. Onishi[*]

Emissions from oil/gas extraction activities in the Arctic are already important in certain regions and may increase as global warming opens up new opportunities for industrial development. Emissions from oil/gas extraction are sources of air pollutants, but large uncertainties exist with regard to their amounts and composition. In this study, we focus on detailed investigation of emissions from oil/gas extraction in the Norwegian Sea combining measurements from the EU ACCESS aircraft campaign in July 2012 and regional chemical transport modeling. The goal is to (1) evaluate emissions from petroleum extraction activities and (2) investigate their impact on atmospheric composition over the Norwegian Sea. Numerical simulations include emissions for permanently operating offshore facilities from two datasets: the TNO-MACC inventory and emissions reported by Norwegian Environment Agency (NEA). It was necessary to additionally estimate primary aerosol emissions using reported emission factors since these emissions are not included in the inventories for our sites. Model runs with the TNO-MACC emissions are unable to reproduce observations close to the facilities. Runs using the NEA emissions more closely reproduce the observations although emissions from mobile facilities are missing from this inventory. Measured plumes suggest they are a significant source of pollutants, in particular NO_x and aerosols. Sensitivities to NO_x and NMVOC emissions show that, close to the platforms, O_3 is sensitive to NO_x emissions and is much less sensitive to NMVOC emissions. O_3 destruction, via reaction with NO, dominates very close to the platforms. Far from the platforms, oil/gas facility emissions result in an average daytime O_3 enhancement of +2% at the surface. Larger enhancements are predicted at noon ranging from +7% at the surface to +15% at 600 m. Black carbon is the aerosol species most strongly influenced by petroleum extraction emissions. The results highlight significant uncertainties in emissions related to petroleum extraction emissions in the Arctic.

Keywords: oil/gas emissions; oil/gas pollution; Norwegian Sea oil/gas extraction; Arctic pollution; air quality modeling

1. Introduction

Modeling and observational studies have shown that sources contributing to Arctic air pollution, namely aerosols and trace gases, are primarily located in the northern mid-latitudes (e.g. Wespes et al. 2012; Shindell et al., 2008; Jacob et al., 2010; Law et al., 2014). Previous work has highlighted the sensitivity of the Arctic climate to short-lived pollutants, such as black carbon and tropospheric ozone (O_3), from mid-latitudes (e.g., Quinn et al., 2008; Serreze and Barry, 2011; Yang et al. 2014) and the impact of soot deposition on snow and ice on surface albedo (e.g., Hansen and Nazerenco, 2004; Flanner et al., 2007, 2009; Jiao et al., 2014). However, the dominance of remote pollution sources may be in the process of changing due to increased access to the Arctic region, associated with climate change leading, for example to reduced sea ice, and economic drivers already resulting in additional shipping and oil-gas exploration extraction

* LATMOS/IPSL, UPMC Univ. Paris 06 Sorbonne Université, UVSQ, CNRS, Paris, FR

† Deutsches Zentrum für Luft- und Raumfahrt (DLR), Institut für Physik der Atmosphäre, 10 Oberpfaffenhofen, DE

‡ University of Vienna, Faculty of Physics, Aerosol Physics and Environmental Physics, Boltzmanngasse 5, A-1090 Vienna, AT

§ TNO Climate, Air and Sustainability, Princetonlaan 6, 3584 CB Utrecht, NL

‖ NUMTECH, 6 allée Alan Turing, CS 60242, 63178 Aubiere, FR

¶ Laboratoire de Météorologie Dynamique, Ecole Polytechnique, 91128 Palaiseau, FR

** Center for International Climate and Environmental Research, Oslo, NO

Corresponding author: P. Tuccella (paolo.tuccella@lmd.polytechnique.fr)

activities in the Arctic (Stephenson et al., 2011; AMAP, 2010). It has been known for some time that certain local sources such as metal smelting are important sources of aerosols, especially sulfate (SO_4^{2-}), in the eastern Arctic (Prank et al., 2010) and more recently, other near Arctic sources have been shown to have an important impact on Arctic air pollution. In particular, Stohl et al. (2013) suggested that Russian flaring emissions associated with oil and gas extraction and seasonally varying domestic combustion emissions (Klimont et al., 2017) may contribute as much as 42% to surface Arctic annual mean black carbon (BC). This is because Arctic surface sites, such as Zeppelin, Alert and Barrow, are sensitive to surface emissions in or near to the Arctic (Hirdman et al., 2010). Inclusion of these emissions in model simulations led to improved model simulations of BC concentrations and its seasonal cycle in the Arctic (Eckhardt et al., 2015). Local emissions from shipping, related to transport of goods, tourism or fishing, have also been shown to be important sources of aerosols and O_3 (Peters et al., 2011; Eckhardt et al., 2013, Marelle et al., 2016). Ødemark et al. (2012) estimated that current petroleum activity may increase summer mean O_3 in Alaska and western Russia by 5%, and shipping may contribute to a seasonal surface O_3 change of 12% along the Norwegian coast and west coast of Greenland. Ødemark et al. (2012) estimated that the annual average radiative impact from air pollutants, normalized to mean column burden enhancements from current Arctic oil/gas and shipping activities, are similar to the global average. BC aerosols and tropospheric O_3 can lead to increased warming locally in the Arctic. Increases in petroleum extraction may have significant impacts on Arctic climate in the future given that estimates suggest that 30% of global undiscovered gas and 13% of oil is north of the Arctic Circle and mostly located offshore (Gautier et al., 2009).

From 1990 to 2004, Arctic oil production took place in western Russia (79%), Alaska (18%), and Norway (3%), whereas gas production was dominated by western Russia (96%) and Alaska (3%) (Peters et al., 2011). However, current air pollutant emissions from activities related to gas and oil extraction are very uncertain in the Arctic where very little independent data is available to validate reported estimates. For example, there is one order of magnitude difference in oil/gas emissions of NMVOCs in the Norwegian Sea in global inventories derived by Peters et al. (2011) and ECLIPSE (Evaluating the Climate and Air Quality ImPacts of Short-livEd Pollutants) (Klimont et al., 2017). Studies in other regions, such as the mid-west in the United States of America (USA), also suggest that inventories underestimate emissions of CH_4 and NMVOCs from oil/gas extraction (e.g., Xiao et al., 2008; Pétron et al., 2012). Activities related to oil/gas extraction produce emissions of carbon dioxide (CO_2), methane (CH_4), nitrogen oxides ($NO + NO_2 = NO_x$), non-methane volatile organic compounds (NMVOCs), carbon monoxide (CO), sulfur dioxide (SO_2) as well as direct emissions of aerosol particulate matter (PM) containing BC and organic aerosols (OA). These emissions can lead to the production of secondary pollutants namely O_3, SO_4^{2-} and secondary organic aerosols (SOA).

Uncertainties in these emissions are due, in part, to the fact that they result from a variety of activities. For example, combustion of fossil fuel for energy production on fixed offshore production installations for heat and light generation, processing and export of hydrocarbons and the treatment and reinjection of water used in the extraction process produces emissions of CO_2, NO_x, SO_2 and CO (UK Oil and Gas, 2015, report available at http://oilandgasuk.co.uk/environment-report.cfm). Natural gas or diesel fuel is used for this purpose although the use of low NO_x turbines can reduce emissions from this source. Flaring, related to maintenance, well testing and safety procedures, and venting, either intentional or as a result of crude oil transfer procedures (e.g. to/from tankers), are also a source of air pollutants. Flaring is highly variable resulting in emissions of aerosols such as BC and trace gases such as CO_2 and NO_x whilst venting of gases leads to emissions of CH_4 and NMVOCs. In a region like the Norwegian continental shelf, combustion from turbines is an important source of CO_2 and NO_x emissions (http://www.npd.no/en/). As well as emissions from fixed facilities, air pollutants are also emitted from mobile installations, such as storage tankers and drilling rigs, which also produce emissions from fuel combustion in their turbines.

In this study, we investigate the impact of pollutant emissions from oil/gas extraction using a combination of regional modeling and analysis of data collected during flights as part of the European Union (EU) Arctic Climate Change and Society (ACCESS) aircraft campaign in July 2012. During this campaign, measurements were taken in the vicinity of extraction installations in the Norwegian Sea (Roiger et al., 2015). We note that these flights represent, to our knowledge, some of the first reported data on pollutant emissions from oil and gas extraction under summertime Arctic conditions. In this study, we use the data to evaluate available emission datasets and estimate the local and regional scale impacts of these emissions on Arctic atmospheric chemical composition and potential implications for regional air quality. We focus primarily on evaluating the impacts of petroleum extraction emissions on O_3 since only rather limited data is available with which to evaluate the model in terms of aerosols. We use a chemical transport model (Weather Research and Forecast coupled with chemistry: WRF-Chem) run at high resolution (2 km) with available point source emissions for production facilities in the Norwegian Sea region. We describe the ACCESS airborne campaign and the WRF-Chem model setup in Section 2 and the emission datasets in Section 3. In Section 4, the ACCESS measurements are used to evaluate the performance of the model simulations and to provide insights into the validity of the emission inventories that are used. The sensitivity of modeled O_3 to NO_x and NMVOC emissions is discussed in Section 5. The impact of oil/gas emissions on regional levels of O_3 and particulate matter (PM) over the Norwegian Sea is discussed in Section 6. The conclusions are given in section 7.

2. Campaign description and model setup

2.1 ACCESS campaign

An overview of the ACCESS aircraft campaign is given in Roiger et al. (2015). For completeness, we briefly describe the details of the ACCESS campaign, conducted in July 2012 using the DLR Falcon-20 aircraft based in northern Norway. The main aim was to collect data on emerging local pollution sources in the Arctic in order to evaluate their impacts on atmospheric composition and on regional air quality and climate. During the campaign, emissions from shipping and oil/gas extraction, as well as pollution plumes transported from metal smelting activities in north-west Russia and from Siberian fires were studied (see Roiger et al., 2015 for further discussion). An analysis of ACCESS flights focusing on ship emissions and their impacts can be found in Marelle et al. (2016). The Falcon-20 was equipped with trace gas (NO_x, SO_2, O_3, and CO) and aerosol instrumentation including total and non-volatile aerosol particle number concentration and accumulation mode refractory black carbon (rBC) mass mixing ratios.

During the ACCESS campaign 2 flights were dedicated to sampling emissions downwind of offshore oil/gas extraction facilities in the Norwegian Sea. The geographic range and tracks of both flights are shown in **Figure 1a**. While the installations that were sampled are south of the Arctic Circle, they are considered to be within the geographic Arctic as defined by the Arctic Council AMAP (Arctic Monitoring and Assessment Programme) which created an area under its Arctic Environmental Protection Strategy, including the Norwegian Sea. The flights took place on 19 and 20 July 2012, in good meteorological conditions with high visibility, and were performed in close collaboration with the Norwegian oil company Statoil (www.statoil.com). The synoptic situation during the flights was dominated by a low-pressure system located to the north of Scandinavia leading to northerly winds close to the Norwegian coast on 19 July 2012. On 20 July 2012, the low-pressure system moved to the northwest, resulting in north-westerly, rather than northerly winds over the Norwegian Sea. These conditions meant that the plume samplings were not influenced by anthropogenic emissions along the Norwegian coast. Further details about the meteorological conditions are given in Roiger et al. (2015).

As shown in **Figure 1b**, the flight on 19 July 2012 was conducted as a survey to sample emissions from a large number of oil and gas production platforms (Kristin, Åsgard A and B, Heidrun and Norne), a storage condensate tanker (Åsgard C), storage tankers (Randgrid and

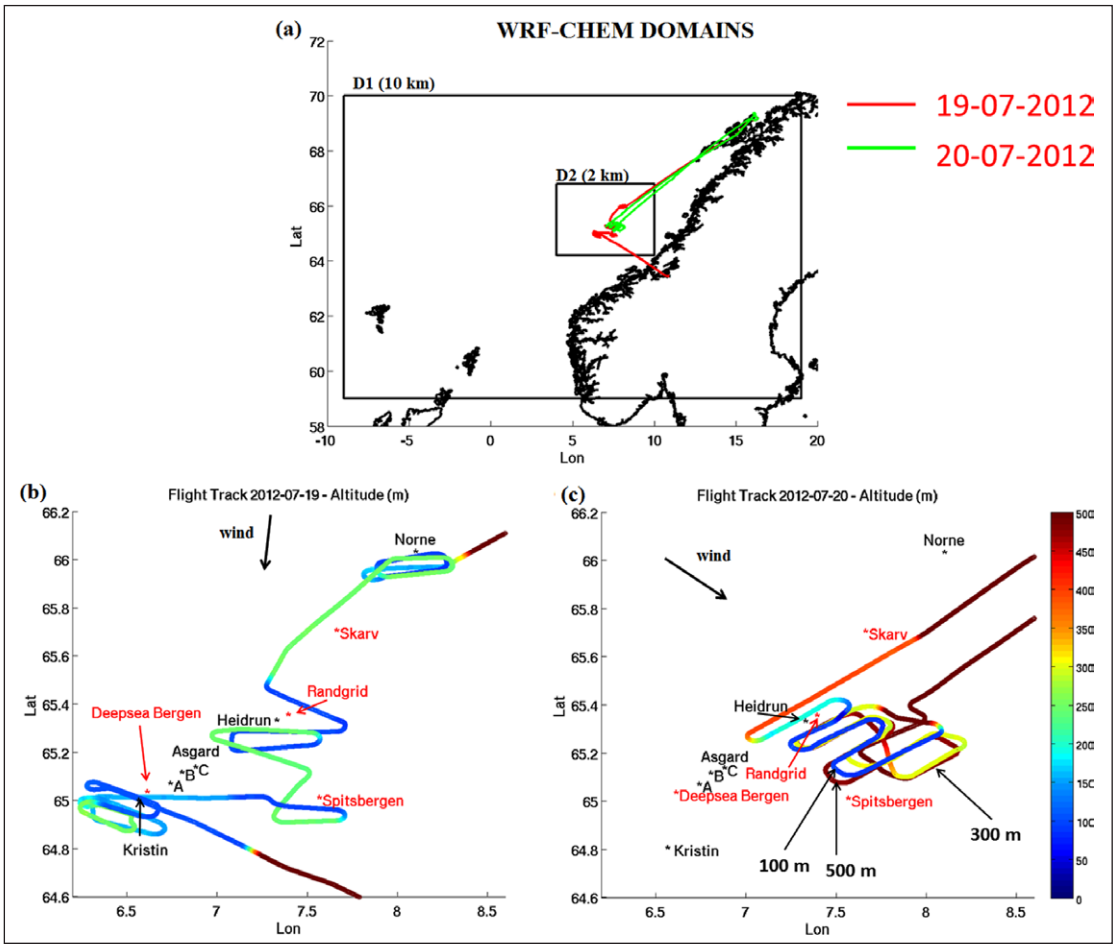

Figure 1: WRF-Chem model domains. Map of WRF-Chem model domains (D1 and D2) with DLR-Falcon flight tracks for the 19 and 20 July 2012 flights **(a)**, and maps of the aircraft altitude during the flights of 19 **(b)** and 20 July **(c)** 2012. See text for details. DOI: https://doi.org/10.1525/elementa.124.f1

Skarv), and drilling rigs (Deepsea Bergen and Transocean Spitsbergen). The flight on 20 July 2012 focused on detailed probing of emissions from the Heidrun production facility using an S-shaped track to sample the plume(s) at various intervals and altitudes (100 m, 300 m and 500 m) downwind as shown in **Figure 1c**. We note that the Norne facility was continuously flaring, on 19 and 20 July 2012, Heidrun was intermittently flaring on both days, whereas Åsgard A was not flaring on 19 July (personal communication, Statoil).

An example of data collected around the platforms is illustrated in **Figure 2**. It shows time series for NO_x, SO_2, nucleation mode aerosols and total non-volatile particle number concentrations measured on the 19 July in plumes downwind of the Åsgard A and B oil production facilities and the condensate storage tanker, Åsgard C. Moderately enhanced levels of nucleation mode aerosols and low levels of SO_2 were observed downwind of Åsgard A and B most likely due to release of VOCs and production of secondary organic aerosols (Roiger et al., 2015). In contrast, particulate matter emissions from the storage tanker Åsgard C were much higher and comprised of non-volatile aerosols. Enhanced SO_2 in plumes from this source points to production of sulfate aerosols and enhancements in BC particles were also noted. NO_x was also higher downwind of this source and other mobile sources (drilling rigs, storage tankers) compared to the fixed production facilities most likely due to combustion emissions. Emissions from drilling rigs (not shown) also contained moderate levels of SO_2, particles, and enhanced BC. These emissions from mobile sources are more characteristic of shipping emissions. Lower NO_x and SO_2 downwind of the production facilities may be due to the use of natural gas for energy production. The ACCESS observations are discussed in more detail in Section 4 when they are used to evaluate the model simulations.

2.2 WRF-Chem model

The impact of emissions from offshore oil/gas installations on air quality in Norwegian Sea was simulated using the WRF-Chem model (version 3.4.1). WRF-Chem is an online model where the physical and chemical processes are fully

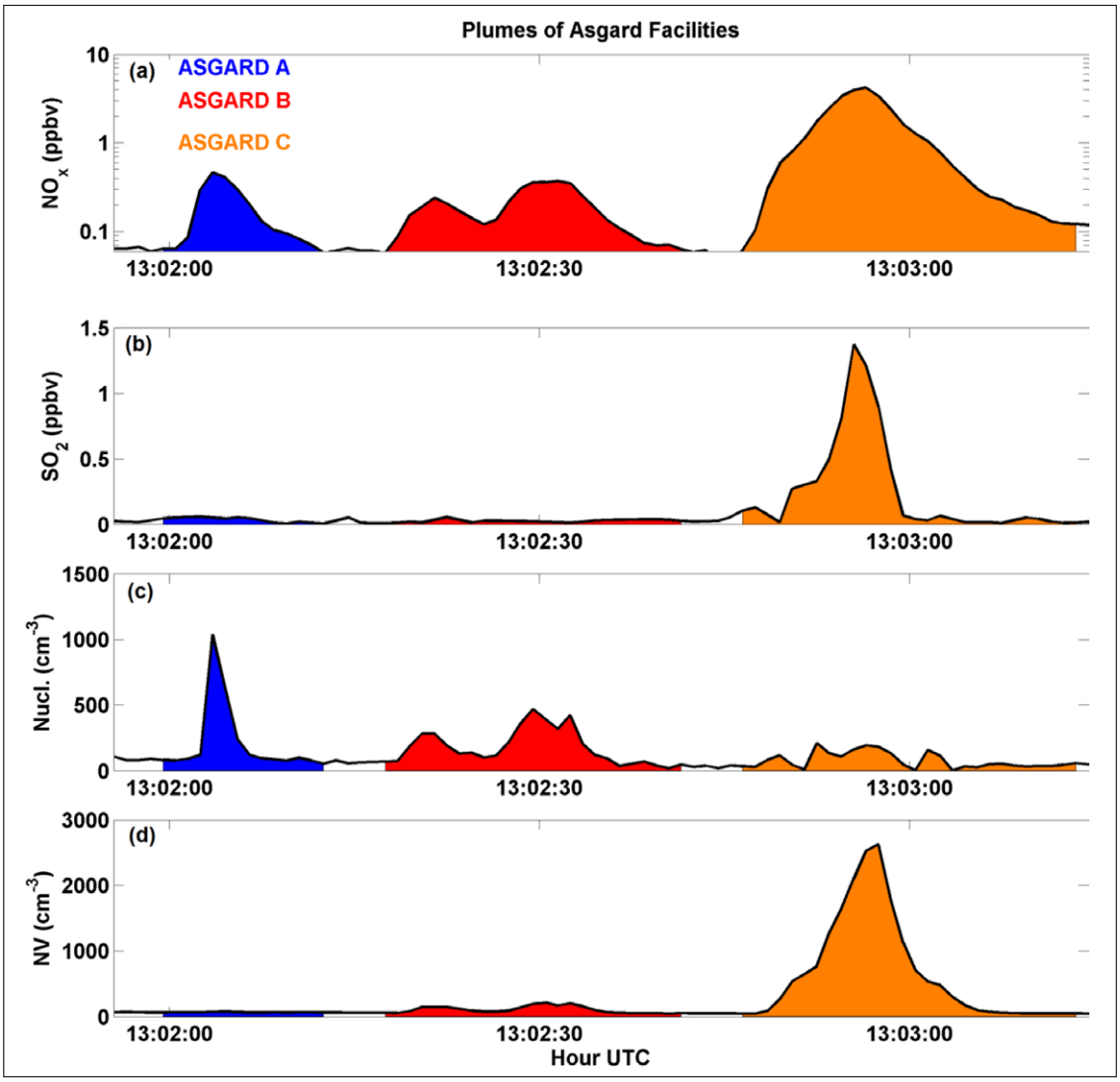

Figure 2: Observed chemical compound composition in the Asgard plume. Observed time series of NO_x (ppbv) **(a)**, SO_2 (ppbv) **(b)**, concentration of nucleation mode particles (cm^{-3}) **(c)**, total non-volatile (NV) particle concentration (cm^{-3}) measured in the plumes of Asgard facilities during the flight of 19 July 2012. DOI: https://doi.org/10.1525/elementa.124.f2

consistent (Grell at al., 2005). The model was run with two 1-way nested domains centered on the Norwegian Sea (see **Figure 1a**) denoted as Domain 1 (D1) and Domain 2 (D2), respectively. The larger outer Domain 1 has 130 × 130 cells and a horizontal resolution of 10 km while the inner nested Domain 2 has 151 × 151 cells with resolution of 2 km. The vertical grid has 33 eta levels up to 50 hPa. The physical and chemical parameterizations used in this work are listed in **Table 1**. Nudging, using meteorological analyses from the European Centre for Medium-range Weather Forecasts (ECMWF) of temperature, water vapor mixing ratio and wind speed, was applied every 6 hours above the planetary boundary layer (PBL) in the outer Domain 1. The choice of this model setup gives the best agreement between meteorological variables and observations collected during ACCESS campaign. The comparison of observed and predicted meteorology is shown in **Figure 3** and will be discussed in the Section 4.

The model was run with the RACM-ESRL gas phase chemical mechanism (Kim et al., 2009), an updated version of the Regional Atmospheric Chemistry Mechanism (RACM) (Stockwell et al., 1997). RACM is a chemical mechanism designed for air pollution studies and includes a full range of photolysis and gas-phase reactions. Aerosol particle dynamics is simulated using the Modal Aerosol and Dynamics for Europe (MADE) scheme (Ackermann et al., 1998). MADE uses three overlapping log-normally distributed modes: Aitken, accumulation and coarse. The

Table 1: WRF-Chem model physical and chemical parameterizations. DOI: https://doi.org/10.1525/elementa.124.t1

Physical process	WRF-Chem Options/Parameterizations
Cloud Microphysics	Morrison (Morrison et al., 2009)
Cumulus	New Grell (G3) (update version of Grell and Devenyi, 2002)
Shortwave radiation	RRTM (Iacono et al., 2008)
Longwave radiation	RRTM (Iacono et al., 2008)
PBL	MYNN (Nakanishi and Niino, 2006)
Surface Layer	Monin-Obukhov
Surface	NOAH LSM (Chen and Dudhia, 2001)
Gas-Phase chemistry	RACM-ESRL (Stockwell et al., 1997; Ahmadov et al., 2012)
Aerosol chemistry	MADE/SOA-VBS (Ackermann et al. 1998; Ahmadov et al., 2012)

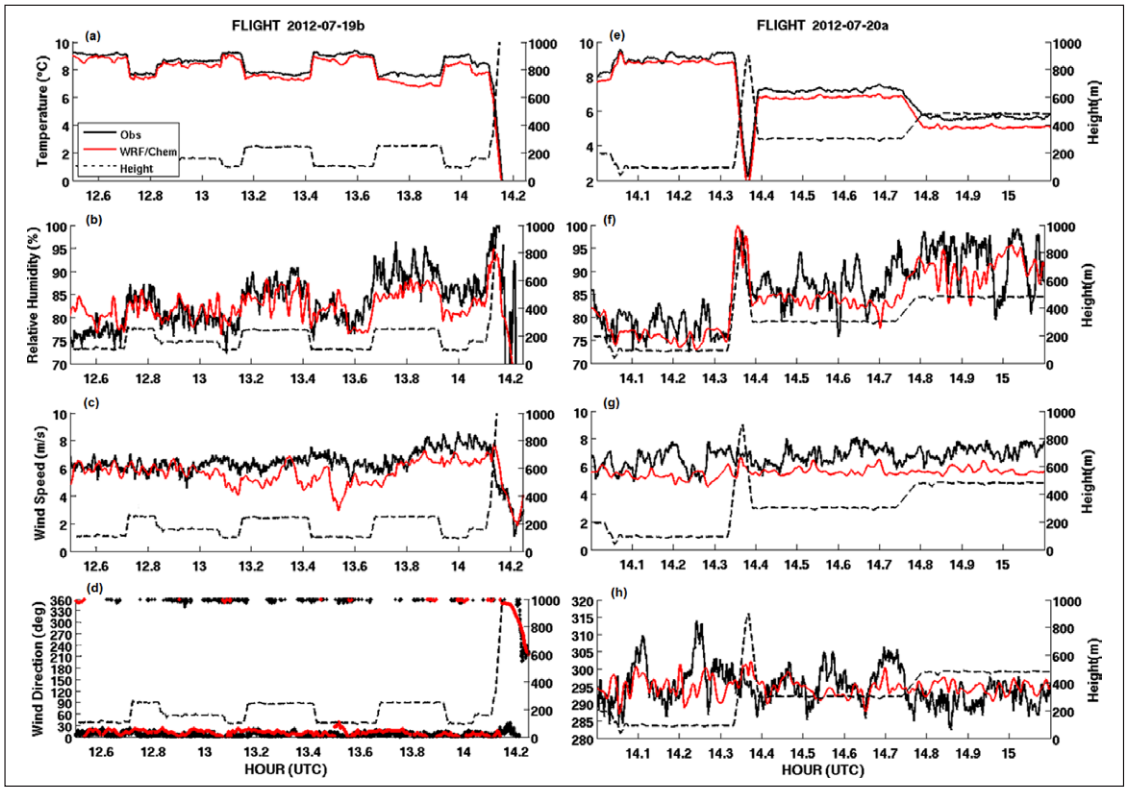

Figure 3: Comparison between observed and modeled meteorology. Time series of observed (black) and simulated (CTRL run, red) temperature **(a, e)**, relative humidity **(b, f)**, wind speed **(c, g)** and wind direction **(d, h)** on 19 (left) and 20 (right) July 2012. DOI: https://doi.org/10.1525/elementa.124.f3

species treated in the Aitken and accumulation modes include inorganic ions, primary particulate matter with aerodynamic diameters less than 2.5 μm ($PM_{2.5}$) that also includes the fine fraction of dust and sea salt, BC, particulate organic matter (POM), SOA, and aerosol water. Unspeciated PM_{10} with aerodynamic diameters less than 10 μm, dust, and sea salt are treated in the coarse mode. SOA production is based on the volatility basis set approach (Ahmadov et al., 2012). Photolysis rates are simulated using the Fast-J scheme (Wild et al., 2000). Dry deposition velocities for trace gases are calculated according to Erisman et al. (1994), while for aerosols the parameterization of Wesely and Hicks (2000) is used. Dry deposition velocities for condensable organic vapors are assumed to be 25% of calculated deposition velocity for HNO_3. Cloud chemistry is treated using the scheme of Walcek and Taylor (1986). Wet deposition from convective updrafts and large scale precipitation is included in the model runs. Aerosol feedbacks on radiation and clouds are not included in these simulations. The tendency terms in the continuity equation are diagnosed following Wong et al. (2009).

WRF-Chem was run over both domains from 14 to 20 July 2012, with 14 to 16 July considered as spin-up for the chemistry. A series of 30 h simulations were performed on each day starting at 00 UTC. The run in the outer Domain 1 was initialized with initial and boundary meteorological conditions provided by ECMWF 6-hourly analyses, at a resolution of 0.125° × 0.125°. Chemical boundary conditions were provided using the output of the global Model for Ozone and Related Chemical Tracers (MOZART) (Emmons et al., 2010) every 6 hours. In order to reproduce background O_3 concentrations outside of plumes, MOZART predicted O_3 values that are used for initial and boundary conditions were multiplied by a factor of 1.1. For the inner Domain 2, initial meteorological conditions as well as meteorological and chemical boundary conditions were taken from the Domain 1 simulations. Due to resolution, the cumulus parameterization was only used in the outer Domain 1. The emissions and simulations performed as part of this study are described in the next section.

3. Emissions and model simulations

In this study, we ran WRF-Chem using available emissions from activities related to oil and gas extraction in the Norwegian Sea. The model was run with anthropogenic emissions taken from TNO-MACC for 2009 (Kuenen et al., 2014) for the larger coarse resolution (Domain 1) simulations, also used as boundary conditions for the high-resolution (2 km) inner Domain 2 simulations. In Domain 2, we used publically reported point source emissions from the Norwegian Environment Agency (NEA) (http://www.norskeutslipp.no/en/Offshore-industry/?SectorID=700) for 2012. We used these emission estimates because the data is provided at high resolution for specific facilities, in contrast to global inventories like Peters et al. (2011) or ECLIPSE (Klimont et al., 2016) that are only available at resolutions larger than 50 km. Nevertheless, it is important to note that emissions for certain storage tankers (Randgrid, Skarv) and drilling rigs (Deepsea Bergen, Transocean Spitzbergen), associated with the offshore industry, are not taken in account in the NEA or TNO-MACC inventories because they are mobile emission sources and/or their emissions are not available. Therefore, in this paper we focus on permanently installed facilities (Heidrun, Norne, Åsgard (A + B + C), Kristin) that were sampled by the ACCESS flights. Note that we used annual average TNO-MACC shipping emissions in all runs (Domains 1 and 2).

The TNO-MACC inventory is a gridded high-resolution (7 × 7 km) regional inventory for Europe providing total annual emissions of NO_x, SO_2, total NMVOC, CH_4, NH_3, CO, and primary aerosols for different Selected Nomenclature for Air Pollutants (SNAP) source sectors (Vestreng, 2003). Emissions are split into area and point sources. Examples of area sources are residential combustion, agriculture and transport sectors, whereas the point sources include power plants, refineries, and major industries such as iron and steel plants (Denier van der Gon et al., 2010). The 2009 emissions for oil and gas extraction facilities in the Norwegian Sea are reported as point sources (SNAP sector 5) and are given in **Table 2**. The TNO-MACC inventory only takes into account emissions of NO_x and NMVOCs from the Åsgard complex, Heidrun, and Norne. It does not report emissions of SO_2, BC, primary PM, or OC from these facilities.

The NEA emissions are provided as point sources for the Åsgard complex (total A + B + C), Heidrun, Norne and Kristin (see **Table 2**). Again, drilling rigs and storage tankers are not included. In the case of the Åsgard complex, made up of 2 production facilities (A, B) and a condensate storage tanker (C), separate emissions for Åsgard A, B, and C were estimated based on ACCESS measurements collected close to and downwind of these facilities on the 19 July 2012 (**Figure 2**). Emissions from each individual installation are given by the product of total emission multiplied by the ratio of the area under each single peak to the total area. The distance between these platforms is sufficient such that mixing of plumes originating from different platforms is unlikely. We make the assumption that plumes from different facilities are independent, and do not consider mixing between plumes. Therefore, the areas below the observed plume peaks shown for NO_x, SO_2 and particles in **Figure 2** are proportional to the emission for each given compound. In the case of NO_x, emissions were split into 6%, 12%, and 82% for Åsgard A, B, and C, respectively. SO_2 was assigned only to Åsgard C because observed SO_2 in Åsgard A and B plumes was under the detection limit of 25 pptv (Roiger et al., 2015). As noted earlier, Åsgard A and B are production facilities emitting negligible SO_2 and non-volatile particles, but a large fraction of nucleation mode particles which could be SOA formed from the nucleation of NMVOCs emitted as a result of venting. In contrast, Åsgard C is a tanker emitting a large amount of SO_2 and non-volatile particles, and a smaller fraction of nucleation mode particles. Therefore, NMVOC emissions were divided by using the observed peak area of nucleation particles as a proxy. Based on these observations, 30%, 47%, and 23% of total NMVOC were attributed to Åsgard A, B, and C, respectively.

Table 2: Total annual emissions from facilities in the Norwegian Sea from the TNO-MACC inventory and reported by the Norwegian Environment Agency (NEA). Aerosol emissions are not included in the inventories and were additionally estimated for the NEA inventory as described in Section 3. DOI: https://doi.org/10.1525/elementa.124.t2

	NO_x (t/y)		NMVOC (t/y)		SO_2 (t/y)		PM (t/y)		EC (t/y)		OC (t/y)	
	TNO	NEA	TNO	NEA	TNO	NEA	TNO	NEA[a)]	TNO	NEA[a)]	TNO	NEA[a)]
Kristin	–	180	57	23	–	4	–	4	–	1	–	1
Åsgard (total)	63	2284	8780	5739	–	239	–	115	–	14	–	15
Åsgard A	–	145	–	1747	–	–	–	3	–	1	–	1
Åsgard B	–	270	–	2675	–	–	–	6	–	2	–	2
Åsgard C	–	1869	–	1317	–	239	–	106	–	11	–	12
Heidrun	61	1775	550	255	–	8	–	38	–	10	–	12
Norne	33	658	560	325	–	5	–	14	–	4	–	4

a) Not taken from NEA but additionally estimated.

The NEA emissions do not include aerosols. Therefore emissions of PM, BC and POC were estimated using emission factors for Norwegian oil/gas operations for 2004 reported by Peters et al. (2011). Emitted aerosol mass was calculated by assuming that it is proportional to NO_x emissions using the ratio between the emission factor of a given aerosol compound and that of NO_x. The values obtained under this assumption are reported in **Table 2**.

In this study, we have used the most relevant emissions estimates for the facilities that were the focus of the measurement campaign. These emissions are available from NEA for the year 2012, which corresponds to the year of the measurement campaign. For regional background emissions, we use the TNO-MACC inventory, which is most recently available for 2009. We also compare model runs using TNO-MACC emissions with the more up to date 2012 NEA emissions for comparison. Several notable differences are apparent between the two inventories used in this study as shown in **Table 2**. TNO-MACC NO_x emissions for the facilities are about 30 times smaller than those from NEA while TNO-MACC NMVOC emissions are about a factor 1.5–2.0 higher than NEA. NEA reporting, which is available yearly, reveals that there were some changes due to inter-annual variability in emissions between 2009 and 2012, especially for NO_x. For example, Heidrun and Norne NO_x emissions were lower by 9% and 37%, and NMVOC emissions by 22% and 2%, respectively in 2012 compared to 2009. In contrast, 2012 emissions from Asgard complex were higher than 2009 by 16% and 2% for NO_x and NMVOC, respectively. These differences in annual amounts, which reflect inter-annual variability in the emissions, are not large enough to account for the differences between TNO-MACC and NEA reported in **Table 2**.

The horizontal and vertical distribution of the emissions, their time variability, NMVOC speciation and aggregation in WRF-Chem model species follows Tuccella et al. (2012). Following this method emissions are distributed over WRF-Chem vertical levels depending on the SNAP sector (Vestreng, 2003). In particular for oil/gas sector (SNAP 5), 90% of emissions are distributed within the first 90 m and 10% between 90 to 170 m. Temporal variability is calculated using generic monthly, weekly, daily and hourly factors derived from Schaap et al. (2005). Following Tuccella et al. (2012), NMVOC emissions are speciated using UK data (Passant, 2002) and aggregated into WRF-Chem species following the reactivity weighting factor principle (Middleton et al., 1990). Following Passant (2002), NMVOC emissions are split into 88% alkanes, 5% alkenes, 0.6% aromatics and 7% are unassigned, i.e. the fraction of compounds in the speciation database whose assignment to a lumped species is difficult or arbitrary. Primary aerosol mass emissions are distributed 10% into Aitken mode and 90% into accumulation mode.

In the reference control run (CTRL), the model was run for the inner Domain 2 using reported NEA emissions and additionally estimated aerosol emissions for the oil/gas production facilities. All other emissions, such as shipping, were from TNO-MACC emissions which were also used in the outer Domain 1. This included shipping emissions and, in the case of Domain 1, all sectors for anthropogenic emissions along the Norwegian coast. For comparison purposes, we also performed a run over Domain 2 using the TNO-MACC emissions, referred to as TNO. In this case, we only used available emissions of NO_x and NMVOCs, i.e. without any estimated aerosol or SO_2 emissions. Based on the differences noted earlier between TNO-MACC and NEA NO_x and NMVOC emission inventories, we examine the sensitivity of model results to levels these emissions in Section 5. The details of all model runs, including the sensitivity tests, are given in **Table 3**.

4. Model evaluation and interpretation of the ACCESS aircraft campaign measurements

In this section, model simulations are evaluated against the ACCESS aircraft campaign data. Results are also used to interpret the measurements collected downwind from the platforms. We focus on the CTRL run simulations in

Table 3: Description of model runs used to study the impact of oil/gas emissions in the high resolution domain (D2).
DOI: https://doi.org/10.1525/elementa.124.t3

Run Name	Description
TNO	Run with TNO emissions (see Table 2)
CTRL	Run with NEA emissions (see Table 2) and estimated aerosol emissions using the emission factors in Peters et al. (2011)
T1	No emissions
T2	CTRL with NO_x facilities emissions doubled
T3	CTRL with NO_x facilities emissions reduced by a factor 2
T4	CTRL with NMVOC emissions increased 5 times

Domain 2 performed at high resolution with NEA and estimated aerosol emissions in order to assess whether the model is able to reproduce pollution plumes from oil/gas production facilities. The results discussed in this section are representative of model behavior in the region close to the facilities and up to 10–30 km downwind.

Correct prediction of meteorology in WRF-Chem is the first step in studying platform emissions where simulation of wind speed and direction is of crucial importance for the correct prediction of plume position and extent. **Figure 3** compares observed and simulated time series of temperature, relative humidity, wind speed and direction along the flight tracks. WRF-Chem underestimates the observed temperature by about 0.5°C and observed relative humidity by 2% on average. Wind speed is underpredicted with a mean bias of ~1 m/s, while the error in the wind direction is on average a few degrees. The errors in modeled temperature and relative humidity may affect the prediction of chemical rates and aerosol formation, whereas discrepancies in simulating wind fields may lead to discrepancies in plume transport, including plume location, pollutant concentrations, and plume dilution, as discussed in the following sections.

Figure 4 shows maps of predicted NO_x and O_3 mixing ratios as well as particle number concentration from the CTRL run at 100 and 300 m on 20 July downwind of Heidrun compared with the aircraft measurements along the flight tracks. We show results for 20 July 2012 because the comparison using a map view on 19 July is more complex due to the sampling of several facilities at several altitudes during this flight (see **Figures 1b** and **1c**). In general, the model captures the overall distribution of the NO_x plumes at all altitudes, but has a tendency to disperse and dilute the peaks over several grid cells, leading to an underestimation of concentrations in some plumes. The absence of emissions in the NEA inventory for the Randgrid storage tanker may also explain part of this underestimation. The simulated width of the plumes is larger than observed which may also be attributed to model resolution. These differences are produced by small differences in simulated wind speeds and wind directions. For example, an error of 1 m/s in predicted wind speed leads to a transport discrepancy of about 8 km over 2 hours, which is roughly the distance found between modeled and measured plumes further downwind from the platforms. Background O_3 is overestimated by +1.5 ppbv (about +6%, the same bias is also found on 19 July). WRF-Chem captures lower O_3 in the plumes but, in general, overestimates the observations. One explanation is that O_3 has not undergone sufficient titration due to the missing NO_x sources from the Randgrid ship. Another reason is the dilution of NO_x in the model, due to model resolution, leads to less efficient titration of O_3. The shift, spread and dilution of the plumes is also found in simulated aerosol particle number. In general, the model predicts higher aerosol numbers than observed as shown in **Figures 4e** and **4f**.

The model was also run using NO_x and NMVOC point source emissions from the TNO-MACC inventory for fixed oil/gas extraction facilities in Domain 2 (run TNO). Results are shown in the Supplementary Material (Figure S1). As noted in Section 3, TNO-MACC NO_x emissions are much lower than the NEA estimates resulting modeled NO_x that is 10–100 times lower than the observations. This, together with the fact that NMVOC emissions are higher in TNO-MACC, leads to an overestimation of O_3 in plumes by about 5 ppbv. These results indicate that model simulations using TNO-MACC emissions, albeit at high resolution (7 km), are unable to represent the composition of plumes resulting from permanent oil/gas extraction installations in the Norwegian Sea.

Figure 5 shows the observed and predicted NO_x time series extracted from the CTRL simulations along the flights on 19 and 20 July. The different facilities were identified using FLEXPART-WRF runs (not shown) (Brioude et al. 2013) and indicate a clear separation between the different plumes. WRF-Chem reproduces the observed peaks of NO_x on 19 July 2012 from Åsgard C, Heidrun and Norne although NO_x mixing ratios downwind of Åsgard C are overestimated by the model. This bias arises from the distribution of the NO_x emissions between Åsgard installations, which was based on the ACCESS observations as described in Section 3. Since, during the measurement period, Åsgard A was on a low production cycle with only one reinjection compressor running (Statoil, pers. communication), the attribution of emissions to Åsgard C could be overestimated. In contrast, the model does not show a systematic bias in reproducing the Norne peaks, which was the only facility that was constantly flaring on 19 July due to a plant trip earlier that day. This may also partly explain the overestimation of NO_x peaks downwind of the Heidrun platform on 19 July. Indeed, the NEA emissions are based on total annual amounts, and

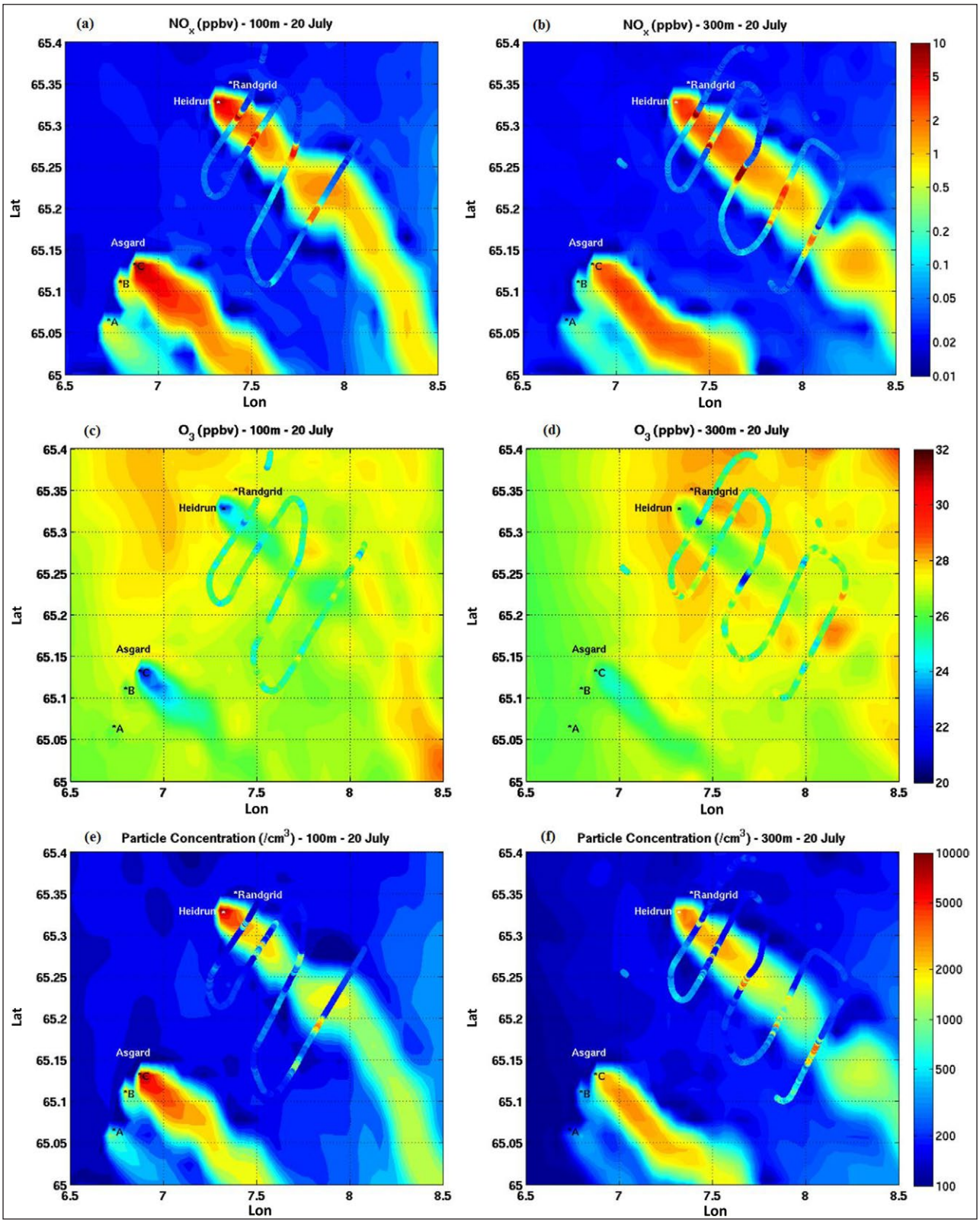

Figure 4: Comparison between observed and modeled NO_x and O_3 on 20 July 2012. Observed (track) and simulated (CTRL run, color shading) NO_x **(a, b)** and O_3 **(c, d)** mixing ratios (ppbv), and particle number concentrations (particle/cm^3) **(e, f)** at 100 (left) and 300 (right) m at 14 UTC on 20 July 2012. DOI: https://doi.org/10.1525/elementa.124.f4

therefore, the emissions implemented in the model are representative of average combustion, flaring and venting activity. Other factors, such as the modeled winds, plume dispersion and lack of emissions from certain drilling ships and storage tankers also impact the model results, as discussed earlier.

Figure 6 shows the comparison between observed and modeled time series of aerosol number concentration.

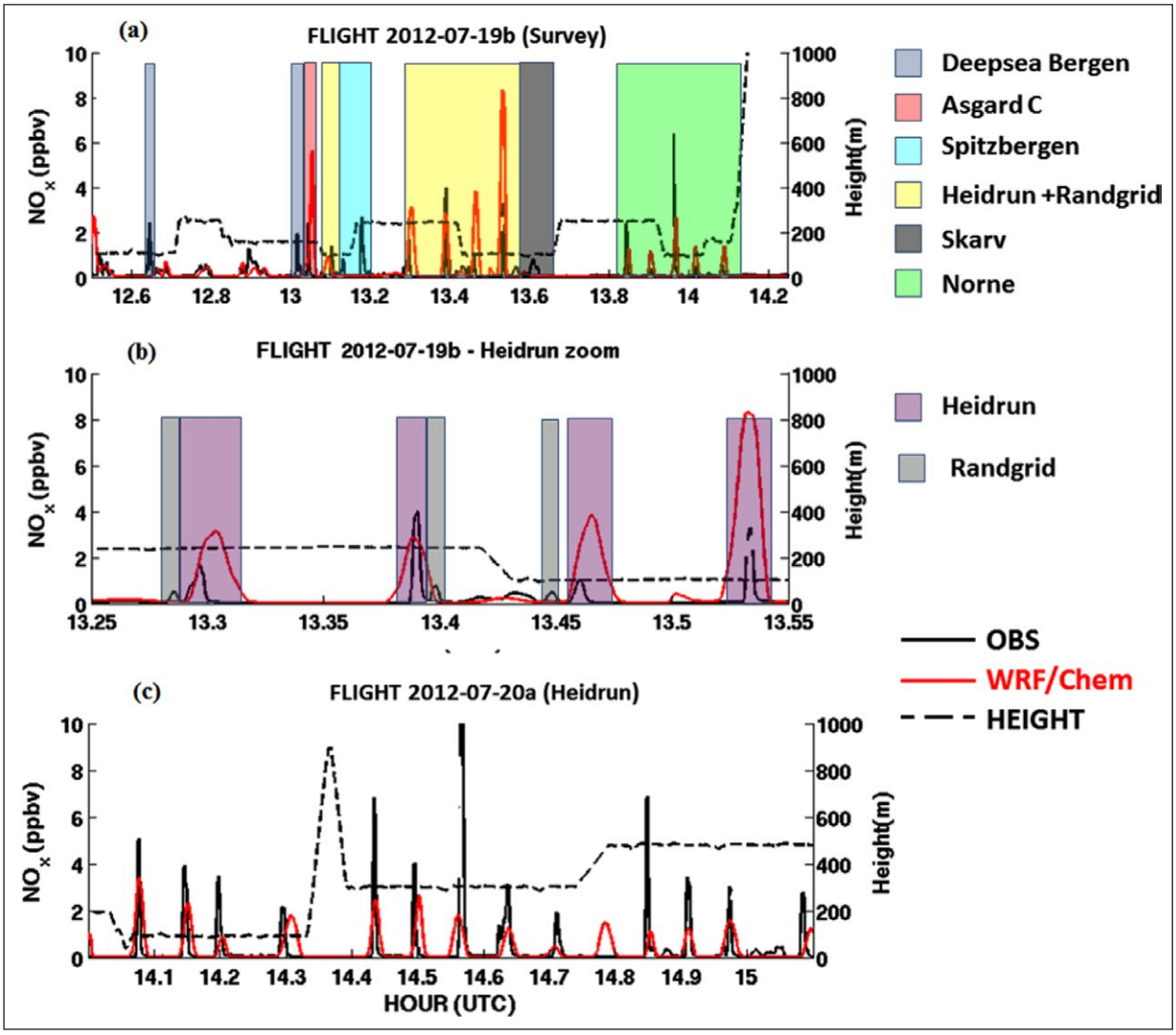

Figure 5: Comparison between observed and modeled NO_x and O_3 on 19 July 2012. Observed (black) and simulated (CTRL run red) time series of NO_x on 19 **(a)** and 20 **(c)** July 2012. The panel **(b)** is a zoom on the Heidrun and Randrid plume of the 19 July. Model simulations included emissions from the Asgard, Heidrun and Norne facilities (see text for details). DOI: https://doi.org/10.1525/elementa.124.f5

The model overestimates the number of aerosol particles in Åsgard C and Heidrun plumes on 19 July, whereas the Norne plume is simulated reasonably well. The Åsgard C bias likely arises from the attribution of all Åsgard SO_2 emissions to the Åsgard C storage tanker and subsequent production of SO_4^{2-} aerosols. Aerosol emissions for other facilities were based on NO_x emissions following Peters et al. (2011) but may include direct particle emissions of, for example, BC, as a result of flaring or combustion as well as production of SOA from NMVOC oxidation as a result of venting. Thus, Heidrun particle numbers may be overestimated because this facility was only intermittently flaring, therefore releasing fewer aerosols into the atmosphere.

The model results for aerosol particle number may also be affected by assumptions made about the emissions and representation of aerosol dynamics in the model. For example, aerosol mass emission in the model is assumed to be distributed 10% in Aitken mode and 90% in the accumulation mode. Also, the standard deviation of the lognormal modes are constant in the aerosol model and may not be representative of the real particle size distribution. Unfortunately, these assumptions could not be verified because measurements of aerosol size distributions were not available. A quantitative analysis of the impact of these assumptions on the results discussed above would require a series of sensitivity tests where the modeled aerosol emission size distribution and standard deviation of the lognormal modes are varied, but this is not the aim of our work. A proper emission size distribution deduced on the basis of the observations could improve the simulation of aerosol particle number concentration but would not eliminate the bias because the correct emission size distribution is a small factor in the prediction of the size distribution, as shown previously by Elleman and Covert (2010). Using a constant standard deviation of lognormal modes could have an impact on the aerosol size distribution especially when the nucleation and growth of aerosol particles is strong (Makkonen et al., 2009) and can

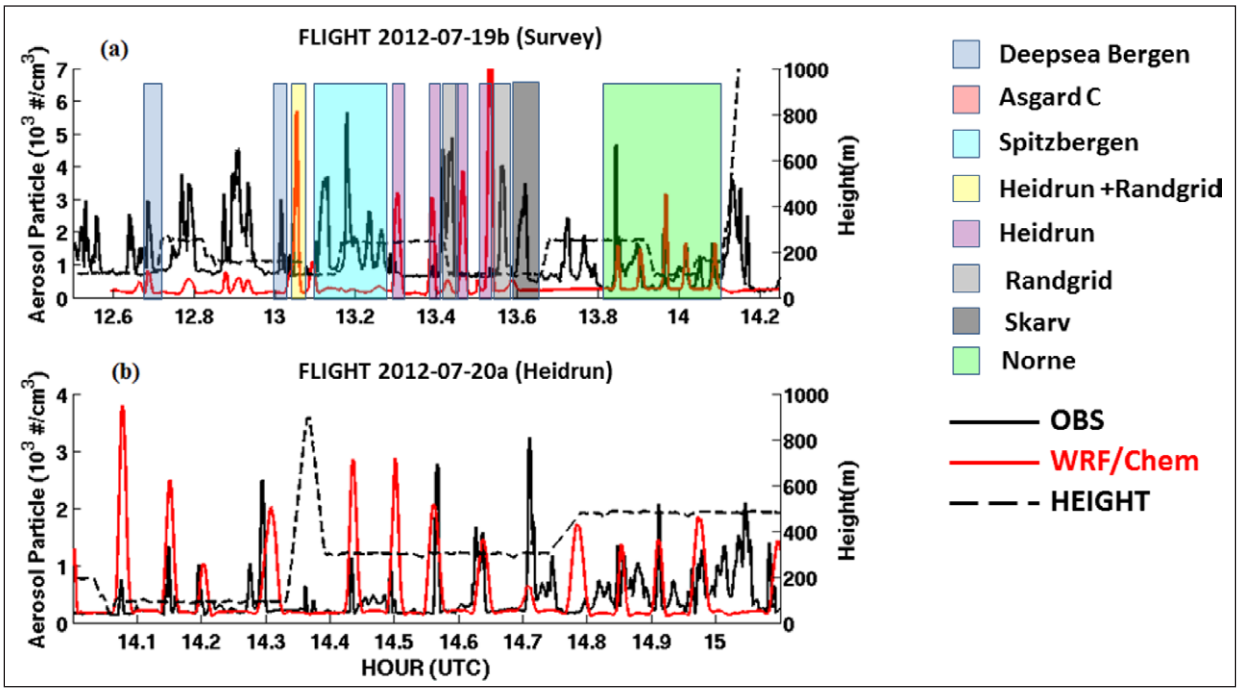

Figure 6: Comparison between observed and modeled particle concentration on 19 and 20 July. Observed (black) and simulated (CTRL run, red) time series of particle concentration on 19 (upper panel) and 20 (bottom) July 2012. Model simulations included emissions from the Asgard, Heidrun and Norne facilities (see text for details). DOI: https://doi.org/10.1525/elementa.124.f6

also affect aerosol loads. For example, Brock et al. (2016) showed that models with constant the standard deviations have larger errors in predicted aerosol optical depths.

Whilst the model results for NO_x and O_3 agree qualitatively with the observations along the flight tracks, such a quantitative evaluation of model performance using point by point comparisons between the model and observations is affected by dilution of concentrations within the model grid and differences in the location of modeled and observed peaks. To overcome this, we also compared pollutant concentrations averaged over modeled and observed plumes. More precisely, the observations were averaged over the time interval where mixing ratios were larger than background concentrations. The model results were averaged over the predicted plumes close to the observed plumes, where modeled values were larger than background mixing ratios. We only used data from 19 July because it is not possible to separate the Heidrun and Randgrid plumes during the flight on 20 July 2012. **Figure 7** shows scatter plots of NO_x and O_3 concentrations averaged over observed and predicted plumes. NO_x is simulated with a correlation of 0.70, a linear regression slope of 1.21, and a bias within a factor of 2. These results show more clearly that WRF-Chem tends to overestimate the values of NO_x close to the facilities, and underestimate NO_x farther away, especially for Heidrun.

O_3 is reproduced less well in the plumes with a correlation of 0.45 although modeled O_3 shows negligible bias for Åsgard C and Heidrun plumes (+0.3%) with respect the observations. The negative O_3 bias in the Heidrun plume is due to biases at low altitudes (less than 100 m) at distances of less than 7 km from the platform where biases reach −10%. Moving away from the installation the model bias is less than 2%. In contrast, simulated O_3 in the Norne plumes is high biased by 1.5 ppbv (+5%). This bias increases further away from the installation ranging from +4% close to up to +8% far from platform. The differences found in the O_3 biases in the predicted plumes are related to different relative amounts of NO_x and NMVOC emitted from different processes. In addition, as discussed previously, many of these processes are intermittent whereas the emission profiles used in the simulations are representative of an average activity. Moreover, significant uncertainties arise from deriving temporal variability in the emissions from an inventory reporting annual totals which are broken down into hourly or daily emissions using generic time profiles. The sensitivity of O_3 to NO_x and NMVOC emissions is investigated in Sections 5 and 6. Model results are also affected by errors in the simulation of wind speed and direction and uncertainties in the emissions although results obtained for simulated NO_x and aerosol particle concentrations suggest that the variations due to errors in simulated wind field are much less than those arising from using the NEA based or TNO-MACC inventories.

5. Sensitivity of modeled O_3 to oil/gas platform emissions

As discussed in Section 4, simulation of modeled O_3 perturbations due to petroleum extraction emissions is dependent on accurate knowledge about these emissions which are highly variable and linked to the various activi-

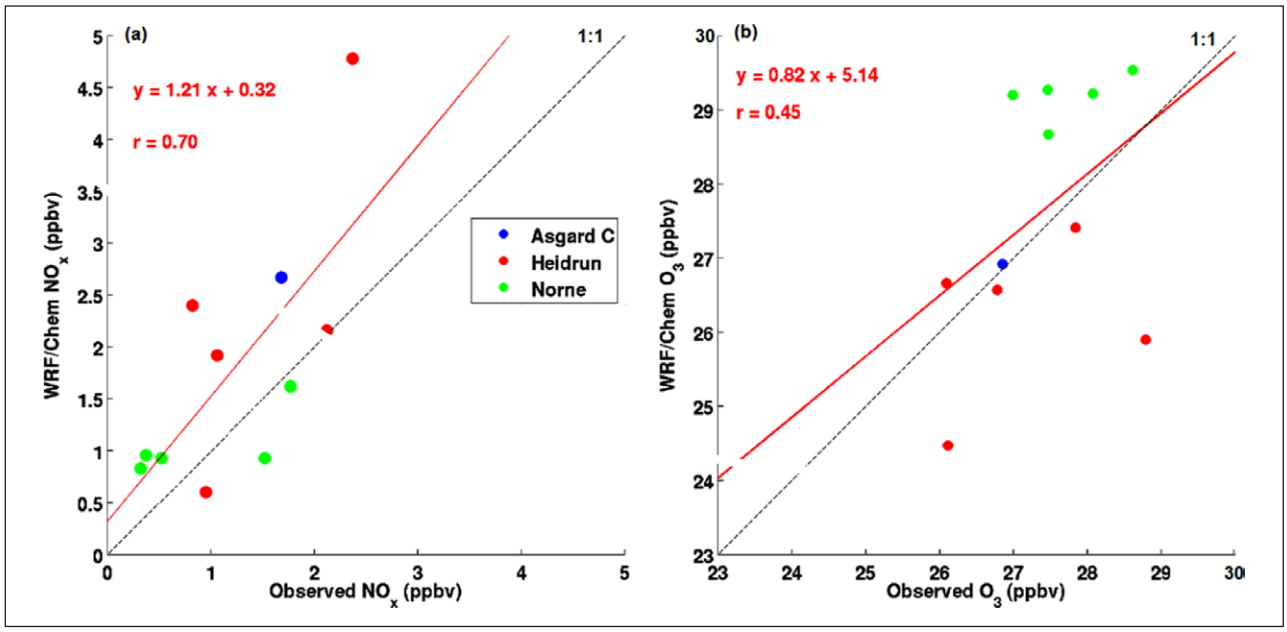

Figure 7: Scatter plot of observed and modelled NO_x and O_3. Scatter plots of observed and modeled (CTRL run) NO_x **(a)** and O_3 **(b)** mixing ratio in the plumes on 19 July 2012. The red lines represent the best least-square linear fit, regression line, 1:1 line, and Pearson's correlation coefficient are also shown. See text for details. DOI: https://doi.org/10.1525/elementa.124.f7

ties on the fixed installations. To investigate the impact of these uncertainties on O_3 close to the facilities, we examine model sensitivity to NO_x and NMVOC emissions by performing a series of runs listed in **Table 3**. Examination of model sensitivity is also driven by the evaluation of model results against the ACCESS observations. In the first sensitivity test (T1) emissions of NO_x and NMVOC were switched off in the CTRL run over Domain 2. For the second (T2) and third (T3) tests we increased (decreased) NO_x emissions by a factor of 2. We also explored the sensitivity of model results to NMVOC emissions since there is a difference of a factor of 1.5 to 2 between NEA and TNO-MACC. In this last test (T4), NMVOC emissions were increased by a factor of 5.

The results are reported in **Table 4** which provides O_3 concentrations averaged over the modeled plumes as a function of distance from the facilities and altitude. Switching off the platform emissions (run T1) almost always leads to higher O_3 concentrations in the plumes compared to the CTRL run, especially close to Heidrun where the enhancement is 3.3 ppbv (+14%) and is the result of less titration by NO_x. Further downwind at 36 km from Heidrun lower emissions results in slightly less O_3 as O_3 production switches from a NO_x-saturated to a NO_x-limited regime. These results suggest that these oil/gas emissions are having a significant impact locally on Arctic boundary layer O_3 in the southern Norwegian Sea. This point is investigated further in the next section. Increasing NO_x emissions by a factor of 2 (run T2) results in lower O_3 in all plumes especially few kilometers downwind the facilities due to increased O_3 titration. O_3 is lower by –6.3% (–1.7 ppbv) for the Åsgard C plume, and reaches 12% (–2.9 ppbv) and –3.5% (–1 ppbv) in the Heidrun and Norne plumes, respectively. Model results are less sensitive to decreasing NO_x emissions by a factor of 2 (run T3) with, in this case, O_3 enhancements that are roughly half those obtained in run T2. For example, O_3 increases by 6.5% (1.7 pbbv) in the plume close to the Heidrun platform. The run T4 with higher NMVOC emissions produces only limited changes in O_3, the largest enhancement 2.6% (0.7 ppbv) being in the Åsgard C plume. These results illustrate the non-linear behavior of O_3 chemistry in remote areas and suggest that modeled O_3 is in a NO_x-satured regime in the plumes up to about 20 km downwind of the platforms. Our results suggest that O_3 production from oil/gas extraction activities in Norwegian Sea is more sensitive to NO_x emissions than NMVOC emissions especially close to the platforms. This sensitivity is generally lower moving away from the platforms (see Section 6). While it is difficult to verify whether the NEA or TNO-MACC NMVOC emissions are more likely to be correct, runs using the TNO-MACC emissions are unable to represent the pollution from oil/gas platforms in the Norwegian Sea, as noted previously.

6. Regional impact of oil/gas emissions on the Norwegian Sea

The discussion so far has been limited to evaluation of model simulations, including the sensitivity to emissions up to 20–30 km downwind of the facilities. Here, we assess local and regional impacts due to oil/gas extraction emissions on O_3 and aerosol distributions in southern Norwegian Sea during July 2012 over scales several 100 km. We examine model results averaged over areas of about 100 km^2 which are comparable to the size of grid cells in global models. Differences between the CTRL run and the run where all O_3 and aerosol precursor emissions were switched off (T1) are used to investigate the contribution of oil/gas extraction to regional pollution. Sensitivities to NO_x and NMVOC emissions are also examined. Model

Table 4: Simulated average O_3 in CTRL run and sensitivity runs (see Table 3). Modeled ozone is averaged over observed plumes along the flight track of 19 July. The units are in ppbv, and the percentages indicate the variation with respect to the CTRL run. The distance from the platforms and altitude where WRF-Chem O_3 is averaged are also reported. DOI: https://doi.org/10.1525/elementa.124.t4

	Distance (km)	Altitude (m)	CTRL (ppbv)	T1 (ppbv)	T2 (ppbv)	T3 (ppbv)	T4 (ppbv)
ÅSGARD C	13	150	26.9	28.6 (+6.3%)	25.2 (–6.3%)	27.9 (+3.7%)	27.6 (+2.6%)
	7	95	24.5	27.8 (+14%)	21.6 (–12%)	26.1 (+6.5%)	24.5 (–)
	7	240	26.6	28.1 (+5.6%)	25.3 (–4.9%)	27.4 (+3.0%)	26.7 (+0.4%)
HEIDRUN	13	95	25.9	27.5 (+6.2%)	24.2 (–6.6%)	26.8 (+3.5%)	26.0 (+0.4%)
	17	240	26.9	27.6 (+3.8%)	25.3 (–4.9%)	27.2 (+2.3%)	26.6 (–)
	36	95	27.4	27.2 (–0.7%)	26.9 (–1.8%)	27.6 (+0.7%)	27.5 (+0.4%)
	1.7	95	28.7	29.6 (+3.1%)	27.7 (–3.5%)	29.1 (+1.4%)	28.7 (–)
	3	240	29.2	29.7 (+1.7%)	28.7 (–1.7%)	29.5 (+1.0%)	29.2 (–)
NORNE	7.3	150	29.2	29.7 (+1.7%)	28.5 (–2.4%)	29.5 (+1.0%)	29.3 (+0.3%)
	10	95	29.3	29.7 (+1.4%)	28.6 (–2.4%)	29.6 (+1.0%)	29.4 (+0.3%)
	10	240	29.5	29.9 (+1.4%)	29.0 (–1.7%)	29.8 (+1.0%)	29.6 (+0.3%)

1. Run with NEA emissions (see Table 2).
2. No emissions.
3. CTRL with NO_x facilities emissions doubled.
4. CTRL with NO_x facilities emissions reduced by a factor 2.
5. CTRL with NMVOC emissions increased 5 times.

diagnosed net photochemical O_3 production rates together with vertical mixing rates are also used to examine processes influencing O_3 distributions.

6.1 Ozone

Figure 8 shows the contribution of oil/gas extraction emissions to surface daytime average O_3, noontime O_3 at 600 m, and daytime average O_3 burdens in the PBL expressed as partial 1000 m columns on the 19 and 20 July. The spatially averaged enhancements downwind of the facilities in the areas A_1 and A_2 shown on **Figure 8** are given in **Tables 5** and **6**. The average impact of oil/gas emissions on O_3 is negative up to 40–50 km downwind of the platforms due to the release of large amounts of NO_x emissions from the facilities. It then becomes positive further downwind from the platforms where lower NO_x concentrations favor photochemical O_3 production. Average daytime O_3 enhancements in areas A_1 and A_2 at the surface (lowest model layer) with respect to background concentrations of 25–30 ppbv are about +2% (+0.6 ppbv) but locally reach +5–7% (+2 ppbv). On both days O_3 enhancements at noon are up to +4 pbbv (+15%) at 600 m and +2 pbbv (+8%) at surface (not shown). The change in the partial column is about +2% (about 2×10^{19} particles/m^2) or 0.07 DU. This result is comparable to the Arctic mean annual change of 0.05 DU due to petroleum extraction activities reported by Odemark et al. (2012) associated with an average radiative forcing of +1.3 mW/m^2.

In order to better understand which chemical and dynamical mechanisms are controlling the local O_3 budget during the summertime Arctic boundary layer the terms of the O_3 continuity equation were analyzed. These include horizontal and vertical advection, net photochemical production rates, and vertical turbulent mixing. In WRF-Chem, dry deposition is included in the vertical mixing term since dry deposition velocity is the boundary condition at surface for the flux of a species. In both the CTRL and T1 runs, background O_3 is dominated by the advection terms with net photochemical production and vertical mixing rates that are 10 times smaller than the advection term. However, O_3 responses to oil/gas emissions are driven by changes in net photochemical production and turbulent mixing plus deposition and differences in the advection terms are not important and are not correlated with emission perturbations. **Figure 9** shows cross sections of the differences (CTRL-T1) in the average daytime net O_3 photochemical production and net vertical mixing terms (both in ppbv/h) extracted along lines C_1 and C_2 shown in **Figure 8**. C_1 is representative of the processes close to the platforms (few kilometers), whereas C_2 represents the behavior far, about 180 km, from the facilities where O_3 column changes are a maximum on 20 July.

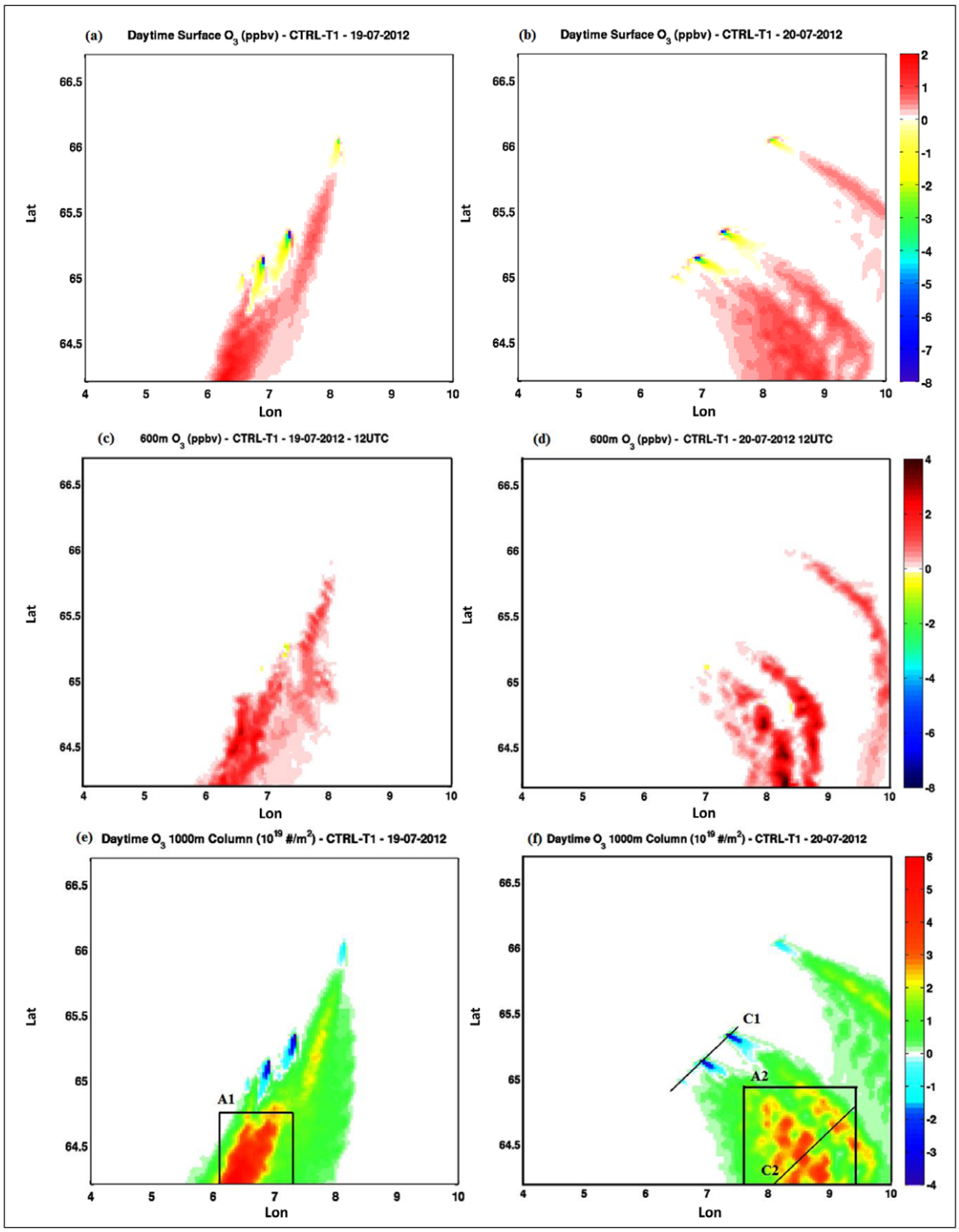

Figure 8: Contribution of oil/gas emissions to O_3 budget. Contribution of oil/gas emissions (calculated as the difference between control run (CTRL) and (T1, no emissions) to surface average day time O_3 **(a, b)**, 600 m O_3 at 12 UTC **(c, d)**, and partial 1000 m column **(e, f)** of average day time ozone on 19 (left) and 20 July 2012. A1 and A2 are the areas used to calculate the average enhancements reported in Tables 5 and 6. C1 and C2 represent the lines used to plot vertical cross sections in Figure 9. DOI: https://doi.org/10.1525/elementa.124.f8

Near the facilities, O_3 is destroyed by photochemistry from the surface up to about 300–400 m. In contrast, O_3 is produced at higher altitudes (300–700 m) but this production is small (0.1 ppbv/h) compared to the destruction rate at lower altitudes of more than 70 ppbv/h locally. In the model, O_3 destroyed near the surface is rapidly replaced by O_3 from higher altitudes by vertical mixing. In **Figure 9**, we note that the difference CTRL-T1 in the vertical mixing rate is negative (downwards) between 200 and 800 m and positive from surface up to 150 m. Net photochemical destruction at the surface is larger than vertical mixing rate, therefore, the net impact of oil/gas emissions on O_3 is negative very close to the platforms. Downwind of the facilities a different behavior is observed. According to the model, O_3 is photochemically produced in the boundary layer reaching maximum average values of up to

Table 5: Contribution from oil/gas extraction emissions to surface O_3 and aerosols. The values are calculated as daytime average for ozone in the area A_1 and A_2 (see Figure 8), and diurnal average for aerosols in the areas A_3 and A_4 (see Figure 10). DOI: https://doi.org/10.1525/elementa.124.t5

Component	19-07-2012	20-07-2012
O_3 (ppbv)	0.6 (2.1%)	0.6 (2.4%)
$PM_{2.5}$ (ng/m³)	20 (3.7%)	10 (1.5%)
POM (ng/m³)	3.9 (8.1%)	2.0 (4.6%)
BC (ng/m³)	2.2 (48%)	1.2 (16%)
Primary $PM_{2.5}$ (ng/m³)	7.8 (11.1%)	4.2 (4.5%)
SO_4^{2-} (ng/m³)	3.9 (2%)	1.8 (0.70%)
SOA (ng/m³)	1.2 (12%)	0.56 (8.8%)

Table 6: As Table 5, but for partial 0–1000 m columns. DOI: https://doi.org/10.1525/elementa.124.t6

Component	19-07-2012	20-07-2012
O_3 (10^{19} #/m²)	2.5 (2.3%)	2.0 (1.9%)
$PM_{2.5}$ (μg/m²)	17 (3.0%)	9.4 (1.2%)
POM (μg/m²)	2.9 (4.7%)	1.6 (2.5%)
BC (μg/m²)	1.8 (35%)	0.94 (15%)
Primary $PM_{2.5}$ (μg/m²)	5.9 (6.7%)	3.3 (2.5%)
SO_4^{2-} (μg/m²)	4.6 (2.1%)	2.6 (0.75%)
SOA (μg/m²)	1.3 (6.9%)	0.67 (4.4%)

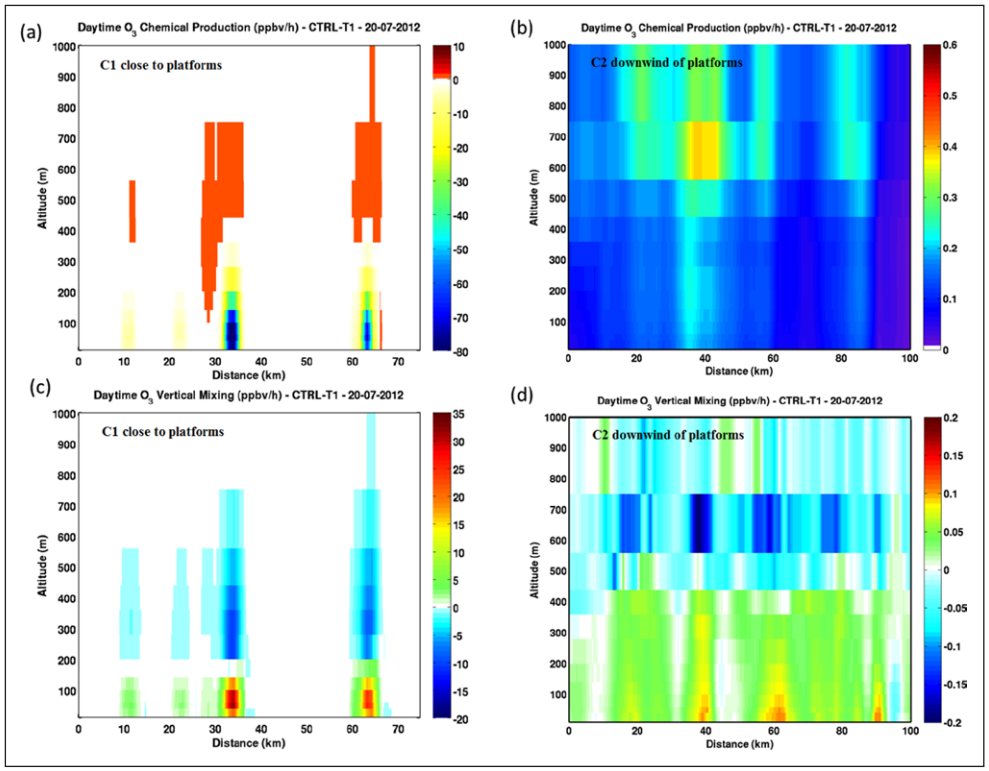

Figure 9: O_3 photochemical production and vertical mixing terms. Cross sections daytime average of the absolute differences (CTRL-T1) in net photochemical O_3 production **(a, c)** and net vertical mixing **(b, d)**. The cross sections are extracted along the lines C1 (left panels) and C2 (right panels) displayed in Figure 8. C1 is representative of the processes close to the facilities, whereas C2 represent the processes far from platforms. DOI: https://doi.org/10.1525/elementa.124.f9

+0.6 ppbv/h at 550–750 m. The difference CTRL-T1 in the vertical mixing tendencies is negative at these altitudes, whereas it is positive close to the surface suggesting that surface O_3 far from platforms is influenced by O_3 transported downwards to the surface by turbulent mixing.

Given that platform emissions are highly uncertain, the sensitivity tests discussed in the previous section can also be used to shed light on the sensitivity of modeled O_3 to NO_x and NMVOC emissions downwind from the facilities. Sensitivity tests show that regional budget of O_3 calculated in areas A_1 and A_2 is sensitive to both NO_x and NMVOC emissions. When NO_x emissions are doubled (T2), surface O_3 within A_1 (19 July) is lower by up to 2 ppbv in plumes downwind of Åsgard and Heidrun, and a weak enhancement of few tenths of ppbv is simulated in the Norne plume. O_3 decreases by up to 1 ppbv since in the run T3 there is not enough NO_x to form O_3. In the sensitivity test T4 where NMVOC emissions were increased by a factor of 5, O_3 is enhanced up to 2 ppbv but only downwind of the Åsgard complex, which are the facilities with the largest release of NMVOCs (see **Table 2**). Changes in the partial columns show a clearer pattern than results at the surface. Increasing or decreasing NO_x (runs T2 and T3) produce similar increases/decreases in O_3 burdens in A1 and A2 of 1–2% while increasing NMVOC emissions by a factor of 5 produces an increase of 2–3% in Asgard C plume. This illustrates that O_3 is less sensitive to NO_x emissions downwind of the platforms and in the case of NMVOC emissions it depends there being sufficient emissions for a particular source.

It is interesting to note differences in terms of amplitude of the response of O_3 to emission variations between our work and other studies examining the impacts of petroleum extraction emissions in other regions of the world. Studies conducted under very different conditions over land in winter in the Uintah Basin (Utah) and Upper Green River Basin (UGRB) (Wyoming) show a wide range of sensitivities in O_3 to emissions. Edwards et al. (2013) and Ahmadov et al. (2015) using box and 3-D models, respectively, showed that O_3 production in Uintah Basin region is sensitive to both NO_x and NMVOC emissions due to the fact that ozone production is at the crossover point between NO_x sensitive and VOC sensitive regimes. Differences between O_3 production in the Uintah Basin and the Norwegian Sea could be due many factors. For example, total NMVOC emissions released in Utah are 30 times larger than those over the Norwegian Sea (for a comparison see **Table 2** of Ahmadov et al. (2015)). Carter and Seinfeld (2012) examined O_3 formation in the UGRB oil/gas production region at two different sites in 2008 and 2011. They showed that, in one case, O_3 production was sensitive to NO_x emissions, whereas in another case it was sensitive to NMVOC emissions. In these studies, net O_3 production was larger than reported here over the Norwegian Sea. However, it should be noted that the studies in Uintah and UGRB basins were conducted under very different atmospheric conditions compared to our study. Significant O_3 production during wintertime episodes was characterized by cold, stagnant conditions, with very shallow boundary layers and snow cover on the ground, while our study was conducted in the near Arctic summer in the Norwegian marine boundary layer. We may expect that emission sensitivities would be different under conditions such as the Arctic winter or spring when temperatures are much colder and boundary layers are shallower. The presence of sea-ice may also play a role since it can affect pollutant concentrations by, for example, modifying of surface albedo, photolysis rates and deposition velocities.

6.2 Particulate matter

Figure 10 displays the contribution of oil/gas emissions to the daytime average $PM_{2.5}$ mass at the surface and to burdens expressed as partial 1 km columns, calculated as the difference between the CTRL run and the run with emissions switched off (T1). The average contributions calculated far from the facilities in the areas A_3 and A_4 (see **Figure 10**) are provided in **Tables 5** and **6**. The largest amount of $PM_{2.5}$, up to 100 ng/m^3, predicted by the model is located close to the platforms.

On 19 July 2012, $PM_{2.5}$ shows relatively small average enhancements (around +3%) in A_3. The average contribution to POM is about +8% at surface and about 5% in the partial 1000 m column. Black carbon is the aerosol species that changes most when oil/gas emissions are included in the simulations with changes at the surface estimated to be +2.2 ng/m^3 (+48%) with increases in the column burden of +1.8 μg/m^2 (+35%). It should be noted that the largest contribution to BC mass is from Åsgard C and Heidrun, the facilities with higher (estimated) BC emissions (see **Table 2**). The average contribution to sulfate is +3.9 ng/m^3 (+2%) at surface and +2.1 μg/m^2 (+2%) in the column, respectively. Predicted sulfate is dominated by Åsgard C emissions which is a condensate storage tanker releasing large amounts of SO_2. Surface and column changes of SOA are estimated to be +12% and 6.9% respectively but SOA mass is very sensitive to NMVOC emissions. Results from the sensitivity test T4 with increased NMVOC emissions produce surface SOA increases of up to 7 ng/m^3 close to the facilities with respect to the CTRL run, with an average enhancement in A_3 of 1.0 ng/m^3 (+7%). Nitrate and ammonium present negligible enhancements. Unspeciated $PM_{2.5}$ increases of 7.8 ng/m^3 (11%) at surface and 5.9 μg/m^2 (7%) in the column. With regard to the vertical distribution of the aerosol (not shown), $PM_{2.5}$ mass change (CTRL-T1) is largest from surface up to about 800 m. Finally, it is interesting to assess the relative contribution of each aerosol species to total mass. The largest contribution to $PM_{2.5}$ is given by SO_4^{2-} (40%). The contribution of POC and unspeciated $PM_{2.5}$ are 10% and 5% respectively, whereas black carbon and SOA are 2% of the total mass.

Aerosol mass enhancements on 20 July, during the flight downwind of Heidrun, are 2–3 times less than those calculated on 19 July (see **Tables 5** and **6**). One factor that may explain these differences is that during 20 July the wind speed in A4 is about 1 m/s larger than in A3 with respect previous day. Moreover the wind direction switched to northwesterly in early morning, whereas it was northerly all day on 19 July. This illustrates the sensitivity of the model results to different meteorological conditions. Specifically, a change in wind speed and direction leads to aerosol mass loads that differ at least by a factor 2.

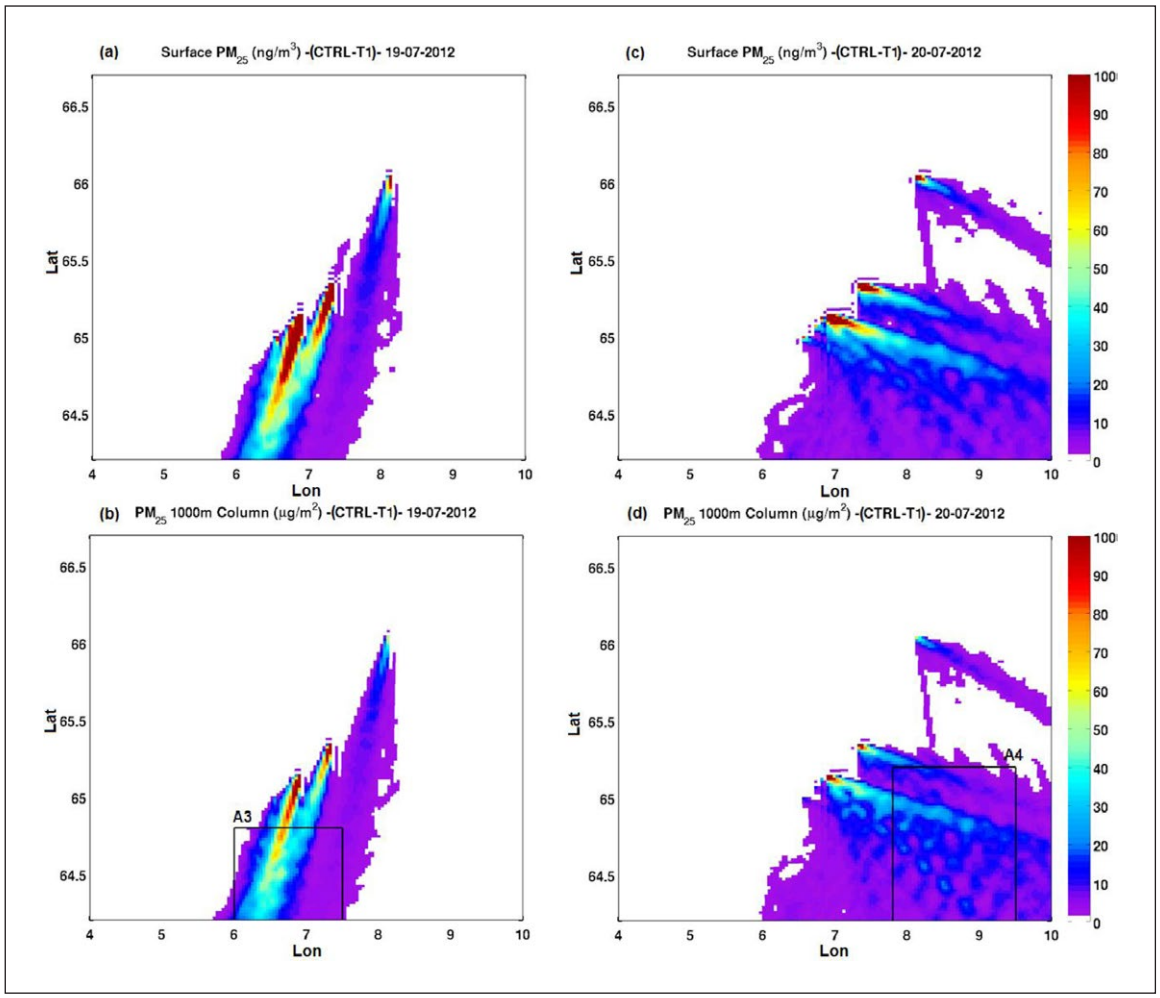

Figure 10: Contribution of oil/gas emissions to $PM_{2.5}$ budget. Contribution of oil/gas emissions (calculated as the difference between control run (CTRL) and (T1, no emissions) to surface $PM_{2.5}$ **(a, c)** and partial 1000 m column **(b, d)** of average diurnal $PM_{2.5}$ on 19 (left) and 20 July 2012. A3 and A4 are the areas used to calculate the average enhancements reported in Tables 5 and 6. DOI: https://doi.org/10.1525/elementa.124.f10

The differences in the columnar aerosol burden between the two days may be explained analyzing the day-to-day variability of wind speed and direction persistence in the two areas A3 and A4. The variability in the wind speed and direction results in more dispersed pollution plumes on the 20 July leading to reduced pollutant concentrations compared to 19 July.

7. Summary and Conclusions

In this work we have presented a study to assess the impact of oil/gas emissions on air pollution during the ACCESS aircraft campaign over the Norwegian Sea in July 2012. The campaign included sampling of pollution plumes from a range of facilities including production platforms, storage tankers, and drilling rigs. Numerical simulations were conducted with the WRF-Chem model using available point source emissions, and model results were evaluated against data collected during the campaign. The sensitivity of O_3 and aerosols to oil/gas emissions was investigated.

Emissions from activities related to oil and gas extraction are highly uncertain and represent a significant source of uncertainty in the assessment of local pollution impacts in the present-day and future Arctic or sub-Arctic regions. In this study, we used two emission estimates (NEA and TNO-MACC) to examine local and regional impacts on atmospheric composition over the Norwegian Sea in July 2012. Large differences were found between the two inventories. NO_x emissions included in TNO-MACC are much smaller compared to Norwegian emissions, by a factor 20–30, whereas the TNO-MACC NMVOC emissions are 1.5–2.0 times larger than the Norwegian NEA data. It is important to note that both inventories do not include aerosol emissions. The emissions of PM, BC and primary OC for NEA were estimated using emission factors for Norwegian Arctic reported by Peters et al. (2011).

Results from a control simulation run with NEA emissions were evaluated using the aircraft measurements. The model was run over a high-resolution domain covering the region of the ACCESS flights allowing assessment of model behavior up to 30 km downwind the facilities. WRF-Chem is able to capture the overall distribution of the plumes of NO_x, O_3, and aerosol particle number concentrations at several altitudes. Nevertheless, predicted plumes are diluted over several grid points, and modeled peaks are not precisely at the position observed. These differences are attributable to the model grid resolution (7 km) and to uncertainties in simulated winds. Simulations with TNO emissions do not reproduce observed NO_x and O_3 with

NO_x being 10–100 times lower than the observations, and O_3 within plumes overestimated by 5 ppbv.

Modeled average NO_x and O_3 concentrations in plumes are reproduced with a correlation coefficient of 0.70 and 0.45, respectively. The bias in predicted O_3 is sensitive to differences in the relative amounts of NO_x and NMVOC emissions, and depends on operational procedures, such as flaring, at different facilities which can be very intermittent. Predicted NO_x and aerosol particles are overestimated in the plumes downwind of facilities that were not flaring, whereas WRF-Chem captures better enhancements downwind of installations that reported normal activity. The emissions are representative of average activity and do not take in account the variations in daily activity of the facilities. The impact of uncertainties in emissions on O_3 levels in the plumes was investigated using sensitivity tests, showing that close to the platforms O_3 is sensitive to NO_x rather than NMVOC emissions. Further downwind, results are sensitive to both NO_x and NMVOC emissions.

In order to assess the wider impact of oil/gas emissions on O_3 and aerosols we compared NEA simulation runs to runs performed without emissions. We find that both aerosols and O_3 are enhanced up to 50 km downwind of the platforms with average daytime enhancements in O_3 of up to +5–7% (+2 ppbv) locally at the surface and larger noontime enhancements of up to 4 ppbv at around 600 m. This represents a significant regional enhancement in O_3 above background concentrations of 25–30 ppbv. These enhancements are due to a switch from net photochemical destruction close to the platforms to net photochemical production accompanied by vertical mixing of O_3 downwind. In terms of aerosols, the largest changes are found in black carbon which increases 2.2 ng/m^3 (+48%) at the surface and +1.8 $\mu g/m^2$ (+35%) in the column due to oil/gas extraction emissions. Primary $PM_{2.5}$, to which $SO4^{2-}$ makes the largest contribution, is enhanced by 7.8 ng/m^3 (11%) at the surface and 5.9 $\mu g/m^2$ (7%) in the column.

Our results indicate the necessity to improve estimates of oil/gas extractions emissions, including their temporal variability and spatial location. In addition, the impact of oil/gas emissions found in this study is likely to be underestimated because emissions from mobile platforms such as storage tankers and drilling rigs are not taken in account in either the NEA or TNO-MACC inventories. At the same time more detailed shipping emissions need to be included. Another significant source of uncertainty is associated with the fact that oil/gas extraction aerosol emissions are not included in current inventories. It is also interesting to note that the Norwegian emissions from oil and gas exploration (SNAP 5) in the TNO-MACC inventory are based on the official Norwegian emissions reporting to EMEP (available at http://www.ceip.at) as reported in 2011. The NEA emissions are apparently not included in the Norwegian reporting to EMEP, at least not at the time of construction of the TNO-MACC inventory by Kuenen et al. (2014). Our analysis suggests that the TNO-MACC inventory does not fully represent the Norwegian offshore Oil and Gas air pollutant emissions. We suggest that a correction in the TNO-MACC data could be made for the emissions from oil and gas exploration in the Norwegian Sea based on the NEA data and information but an additional effort will be needed for the PM emissions which were also lacking in NEA.

We note also that, in this study, the impact of petroleum extraction emissions on pollutant concentrations has been calculated based on a rather short time period covering the ACCESS campaign. More accurate regional assessment would require simulations on time scales of several months, which is not the focus of the present study. Impacts may also be larger at other times of year, in particular, in winter or spring when it is expected that boundary layer depths are shallower and different chemical processes may operate due less sunlight, lower temperatures, etc.. Future exploration in the Arctic may also take place in regions with sea-ice or snow which could also have an impact on the chemical and dynamical processing of these emissions.

The results obtained in this study point to the need for further work to assess emerging air quality and climate impacts due to oil/gas emissions in the Arctic and demonstrate that improvements in current emission inventories and knowledge of processes are required in order to take in account all the various types of emissions associated with oil/gas extraction and production. For this purpose further intensive campaigns including measurements of NMVOCs, aerosol size distributions and composition, are desirable in the Arctic oil/gas extraction regions, such as northern Russia, where substantial oil/gas extraction is already occurring. In this study we have focused on the local scale impacts of these emissions. In the future, more accurate and exhaustive evaluation of oil/gas emissions impacts and their radiative forcing are desirable on regional scales.

Data Accessibility Statement

Accessibility to the ACCESS aircraft data can be provided upon request to Anke.Roiger@dlr.de. The TNO emission inventory is available upon request to H. A. C. Denier van der Gon (hugo.deniervandergon@tno.nl), while NEA emissions are freely available online (http://www.norskeutslipp.no/en/Offshore-industry/?SectorID=700).

Supplemental File

The supplemental file for this article can be found as follows:

- **Figure S1.** Comparison between observed and modeled NO_x and O_3 on 20 July 2012.
  DOI: https://doi.org/10.1525/elementa.124.s1

Acknowledgements

The authors are grateful to the DLR flight department for their support during campaign, and to the Statoil company for providing the information about the operational activity of the facilities.

Funding information

The work presented here was funded from the European Union under Grant Agreement n° 265863-ACCESS (http://www.access-eu.org) within the Ocean of Tomorrow call of

the European Commission Seventh Framework Programme. This work benefited from access to IDRIS HPC resources (GENCI: Grand Équipement National de Calcul Intensif, allocations 2014-017141, 2015-017141 and 2016-017141) and the IPSL mesoscale computing center (CICLAD: Calcul Intensif pour le Climat, l'Atmosphère et la Dynamique). French authors also acknowledge funding from the CNRS Chantier Arctique PARCS (Pollution in the Arctic System) project.

Competing interests

The authors have no competing interests to declare.

Author contributions

- Performed model simulations: PT
- Contributed to conception and design: PT, JLT, KSL
- Contributed to acquisition of data: JLT, KSL, JCR, LM, AR, BW, HS, TO
- Contributed to analysis and interpretation of data: PT, JLT, KSL, JCR, HACDG
- Drafted and/or revised the article: PT, JLT, KSL, JCR, AR, HACDG
- Approved the submitted version for publication: PT, JLT, KSL, JCR, LM, AR, BW, HACDG, HS, TO

References

Ackermann, IJ, Hass, H, Memmesheimer, Ebel, A, Binkowski, FS and **Shankar, U** 1998 Modal aerosol dynamics model for Europe: Development and first allpications, *Atmos. Environ.,* **32**(17): 2981–2999. DOI: https://doi.org/10.1016/S1352-2310(98)00006-5

Ahmadov, R, McKeen, SA, Robinson, A, Bahreini, R, Middlebrook, A, de Gouw, J, Meagher, J, Hsie, E, Edgerton, E, Shaw, S and **Trainer, M** 2012 A volatility basis set model for summertime secondary organic aerosols over the eastern United States in 2006, *J. Geophys. Res.,* **117**(D06): 301. DOI: https://doi.org/10.1029/2011JD016831

Ahmadov, R, McKeen, S, Trainer, M, Banta, R, Brewer, A, Brown, S, Edwards, PM, de Gouw, JA, Frost, GJ, Gilman, J, Helmig, D, Johnson, B, Karion, A, Koss, A, Langford, A, Lerner, B, Olson, J, Oltmans, S, Peischl, J, Pétron, G, Pichugina, Y, Roberts, JM, Ryerson, T, Schnell, R, Senff, C, Sweeney, C, Thompson, C, Veres, PR, Warneke, C, Wild, R, Williams, EJ, Yuan, B and **Zamora, R** 2015 Understanding high wintertime ozone pollution events in an oil- and natural gas-producing region of the western US, *Atmos. Chem. Phys*, **15**: 411–429. DOI: https://doi.org/10.5194/acp-15-411-2015

AMAP: Assessment 2007 Oil and Gas in the Arctic: Effects and Potential effects, Arctic Monitoring and Assessment Program (AMAP), Oslo, Norway, 2010.

Brock, CA, Wagner, NL, Anderson, BE, Beyersdorf, A, Campuzano-Jost, P, Day, DA, Diskin, GS, Gordon, TD, Jimenez, JL, Lack, DA, Liao, J, Markovic, MZ, Middlebrook, AM, Perring, AE, Richardson, MS, Schwarz, JP, Welti, A, Ziemba, LD and **Murphy, DM** 2016 Aerosol optical properties in the southeastern United States in summer – Part 2: Sensitivity of aerosol optical depth to relative humidity and aerosol parameters, *Atmos. Chem. Phys*, **16**: 5009–5019. DOI: https://doi.org/10.5194/acp-16-5009-2016

Carter, WPL and **Seinfeld, JH** 2012 Winter ozone formation and VOC incremental reactivities in the Upper Green River Basin of Wyoming, *Atmos. Environ*, **50**: 255–266. DOI: https://doi.org/10.1016/j.atmosenv.2011.12.025

Chen, F and **Dudhia, J** 2001 Coupling an advanced land-surface/hydrology model with the Penn State/NCAR MM5 modeling system, Part I: Model description and implementation, *Mon. Weather Rev,* **129**: 569–585. DOI: https://doi.org/10.1175/1520-0493

Denier van der Gon, HAC, Visschedijk, A, Van der Brugh, H and **Dröge, R** 2010 A high resolution European emission database for the year 2005, a contribution to the UBA-project PAREST: Particle Reduction Strategies, TNO report TNO-034-UT-2010-01895_RPT-ML, Utrecht.

Eckhardt, S, Hermansen, O, Grythe, H, Fiebig, M, Stebel, K, Cassiani, M, Baecklund, A and **Stohl, A** 2013 The influence of cruise ship emissions on air pollution in Svalbard – a harbinger of a more polluted Arctic? *Atmos. Chem. Phys*, **13**: 8401–8409. DOI: https://doi.org/10.5194/acp-13-8401-2013

Edwards, PM, Young, CJ, Aikin, K, deGouw, J, Dubé, WP, Geiger, F, Gilman, J, Helmig, D, Holloway, JS, Kercher, J, Lerner, B, Martin, R, McLaren, R, Parrish, DD, Peischl, J, Roberts, JM, Ryerson, TB, Thornton, J, Warneke, C, Williams, EJ and **Brown, SS** 2013 Ozone photochemistry in an oil and natural gas extraction region during winter: simulations of a snow-free season in the Uintah Basin, Utah, *Atmos. Chem. Phys*, **13**: 8955–8971. DOI: https://doi.org/10.5194/acp-13-8955-2013

Elleman, RA and **Covert, DS** 2010 Aerosol size distribution modeling with the Community Multiscale Air Quality modeling system in the Pacific Northwest: 3. Size distribution of particles emitted into a mesoscale model, *J. Geophys. Res*, **115**: D03204. DOI: https://doi.org/10.1029/2009JD012401

Emmons, LK, Walters, S, Hess, PG, Lamarque, J-F, Pfister, GG, Fillmore, D, Granier, C, Guenther, A, Kinnison, D, Laepple, T, Orlando, J, Tie, X, Tyndall, G, Wiedinmyer, C, Baughcum, SL and **Kloster, S** 2010 Description and evaluation of the Model for Ozone and Related chemical Tracers, version 4 (MOZART-4), *Geosci. Model Dev*, **3**: 43–67. DOI: https://doi.org/10.5194/gmd-3-43-2010

Erisman, JW, Vanpul, A and **Wyers, P** 1994 Parametrization of surfaceresistance for the quantification of atmospheric deposition of acidifying pollutants and ozone, *Atmos. Environ*, **28**(16): 2595–2607. DOI: https://doi.org/10.1016/1352-2310(94)90433-2

Flanner, MG, Zender, CS, Hess, PG, Mahowald, NM, Painter, TH, Ramanathan, V and **Rasch, PJ** 2009 Springtime warming and reduced snow cover from carbonaceous particles, *Atmos. Chem. Phys*, **9**: 2481–2497. DOI: https://doi.org/10.5194/acp-9-2481-2009

Flanner, MG, Zender CS, Randerson, JT and **Rasch, PJ** 2007 Present-day climate forcing and response from black carbon in snow, *J. Geophys. Res*, **112**(D11): 202. DOI: https://doi.org/10.1029/2006JD008003

Gautier, DL, Bird, KJ, Charpentier, RR, Grantz, A, Houseknecht, DW, Klett, TR, Moore, TE, Pitman, JK, Schenk, CJ, Schuenemeyer, JH, Sorensen, K, Tennyson, ME, Valin, ZC and **Wandrey, CJ** 2009 Assessment of undiscovered oil and gas in the Arctic, *Science*, **324**: 1175. DOI: https://doi.org/10.1126/science.1169467

Grell, GA and **Devenyi, D** 2002 A generalized approach to parameterizing convection combining ensemble and data assimilation techniques, *Geophys. Res. Lett*, **29**(14): p. 38. DOI: https://doi.org/10.1029/2002GL015311

Grell, GA, Peckham, SE, Schmitz, R, McKeen, SA, Frost, G, Skamarock, WC and **Eder, B** 2005 Fully coupled 'online' chemistry in the WRF model. *Atmos. Environ*, **39**: 6957–6976. DOI: https://doi.org/10.1016/j.atmosenv.2005.04.027

Hansen, J and **Nazarenko, L** 2004 Soot climate forcing via snow and ice albedos, *P. Natl. Acad. Sci. USA*, **101**: 423–428. DOI: https://doi.org/10.1073/pnas.2237157100

Hirdman, D, Sodemann, H, Eckhardt, S, Burkhart, JF, Jefferson, A, Mefford, T, Quinn, PK, Sharma, S, Ström, J and **Stohl, A** 2010 Source identification of short-lived air pollutants in the Arctic using statistical analysis of measurement data and particle dispersion model output, *Atmos. Chem. Phys*, **10**: 669–693. DOI: https://doi.org/10.5194/acp-10-669-2010

Iacono, MJ, Delamere, JS, Mlawer, EJ, Shephard, MW, Clough, SA and **Collins, WD** 2008 Radiative forcing by long-lived greenhouse gases: Calculations with the AER radiative transfer models, *J. Geophys. Res*, **113**(D13): 103. DOI: https://doi.org/10.1029/2008JD009944

Jacob, DJ, Crawford, JH, Maring, H, Clarke, AD, Dibb, JE, Emmons, LK, Ferrare, RA, Hostetler, CA, Russell, PB, Singh, HB, Thompson, AM, Shaw, GE, McCauley, E, Pederson, JR and **Fisher, JA** 2010 The Arctic Research of the Composition of the Troposphere from Aircraft and Satellites (ARCTAS) mission: design, execution, and first results, *Atmos. Chem. Phys*, **10**: 5191–5212. DOI: https://doi.org/10.5194/acp-10-5191-2010

Jiao, C, Flanner, MG, Balkanski, Y, Bauer, SE, Bellouin, N, Berntsen, TK, Bian, H, Carslaw, KS, Chin, M, De Luca, N, Diehl, T, Ghan, SJ, Iversen, T, Kirkevåg, A, Koch, D, Liu, X, Mann, GW, Penner, JE, Pitari, G, Schulz, M, Seland, Ø, Skeie, RB, Steenrod, SD, Stier, P, Takemura, T, Tsigaridis, K, van Noije, T, Yun, Y and **Zhang, K** 2014 An AeroCom assessment of black carbon in Arctic snow and sea ice, *Atmos. Chem. Phys*, **14**: 2399–2417. DOI: https://doi.org/10.5194/acp-14-2399-2014

Kim, SW, Heckel, A, Frost, GJ, Richter, A, Gleason, J, Burrows, JP, McKeen, S, Hsie, EY, Granier, C and **Trainer, M** 2009 NO_2 columns in the western United States observed from space and simulated by a regional chemistry model and their implications for NO_x emissions, *J. Geophys. Res. Atmos*, **114**: D11301. DOI: https://doi.org/10.1029/2008JD011343

Klimont, Z, Hoglund, L, Heyes, Ch, Rafaj, P, Schoepp, W, Cofala, J, Borken-Kleefeld, J, Purohit, P, Kupianen, K, Winiwarter, W, Amann, M, Zhao, B, Wand, SX, Bertok, I and **Sander, R** 2016 Global scenarios of air pollution and methane: 1990–2050, in preparation.

Kuenen, JJP, Visschedijk, AJH, Jozwicka, M and **Denier van der Gon, HAC** 2014 TNO-MACC_II emission inventory: a multi-year (2003–2009) consistent high-resolution European emission inventory for air quality modelling, *Atmos. Chem. Phys. Discuss*, **14**: 5837–5869. DOI: https://doi.org/10.5194/acpd-14-5837-2014

Law, KS, Stohl, A, Quinn, PK, Brock, C, Burkhart, J, Paris, J-D, Ancellet, G, Singh, HB, Roiger, A, Schlager, H, Dibb, J, Jacob, DJ, Arnold, SR, Pelon, J and **Thomas, JL** 2014 Arctic Air Pollution: New Insights From POLARCAT-I PY, *Bull. Amer. Meteor. Soc.* DOI: https://doi.org/10.1175/BAMS-D-13-00017.1

Makkonen, R, Asmi, A, Korhonen, H, Kokkola, H, Järvenoja, S, Räisänen, P, Lehtinen, KEJ, Laaksonen, A, Kerminen, V-M, Järvinen, H, Lohmann, U, Bennartz, R, Feichter, J and **Kulmala, M** 2009 Sensitivity of aerosol concentrations and cloud properties to nucleation and secondary organic distribution in ECHAM5-HAM global circulation model, *Atmos. Chem. Phys*, **9**: 1747–1766. DOI: https://doi.org/10.5194/acp-9-1747-2009

Marelle, L, Thomas, JL, Raut, J-C, Law, KS, Jalkanen, J-P, Johansson, L, Roiger, A, Schlager, H, Kim, J, Reiter, A and **Weinzierl, B** 2016 Air quality and radiative impacts of Arctic shipping emissions in the summertime in northern Norway: from the local to the regional scale, *Atmos. Chem. Phys*, **16**: 2359–2379. DOI: https://doi.org/10.5194/acp-16-2359-2016

Middleton, P, Stockwell, WR and **Carter, WP** 1990 Aggregation and analysis of volatile organic compound emissions for regional modelling, *Atmos. Environ*, **24**: 1107–1133. DOI: https://doi.org/10.1016/0960-1686(90)90077-Z

Morrison, H, Thompson, G and **Tatarskii, V** 2009 Impact of cloud microphysics on the development of trailing stratiform precipitation in a simulated squall line: comparison of one- and two-moment scheme, *Mon. Weather Rev*, **137**: 991–1007. DOI: https://doi.org/10.1175/2008MWR2556.1

Nakanishi, M and **Niino, H** 2006 An improved Mellor-Yamada Level-3 Model: its numerical stability and application to a regional prediction of advection fog, *Bound.-Lay. Meteorol*, **119**: 397–407. DOI: https://doi.org/10.1007/s10546-005-9030-8

Ødemark, K, Dalsøren, SB, Samset, BH, Berntsen, TK, Fuglestvedt, JS and **Myhre, G** 2012 Short-lived

climate forcers from current shipping and petroleum activities in the Arctic, *Atmos. Chem. Phys*, **12**: 1979–1993. DOI: https://doi.org/10.5194/acp-12-1979-2012

Passant, N 2002 Speciation of UK emissions of NMVOC, AEAT/ENV/0545, AEA Technology, London.

Peters, GP, Nilssen, TB, Lindholt, L, Eide, MS, Glomsrød, S, Eide, LI and **Fuglestvedt, JS** 2011 Future emissions from shipping and petroleum activities in the Arctic, *Atmos. Chem. Phys*, **11**: 5305–5320. DOI: https://doi.org/10.5194/acp-11-5305-2011

Pétron, G, Frost, G, Miller, BR, Hirsch, AI, Montzka, AE, Karion, A, Trainer, M, Sweeney, C, Andrews, AE, Miller, L, Kofler, J, Bar-Ilan, A, Dlugokencky, EJ, Patrik, L, Moore Jr, CT, Ryerson, TB, Siso, C, Kolodzey, W, Lang, PM, Conway, T, Novelli, P, Masarie, K, Hall, B, Guenther, D, Kitzis, DF, Miller, J, Welsh, D, Wolfe, D, Neff, W and **Tans, P** 2012 Hydrocarbon emissions characterization in the Colorado Front Range: A pilot study, *J. Geophys. Res*, **117**. DOI: https://doi.org/10.1029/2011JD016360

Prank, M, Sofiev, M, Denier van der Gon, HAC, Kaasik, M, Ruuskanen, TM and **Kukkonen, J** 2010 A refinement of the emission data for Kola Peninsula based on inverse dispersion modelling. *Atmos. Chem. Phys*, **10**: 10849–10865. DOI: https://doi.org/10.5194/acp-10-10849-2010

Quinn, PK, Bates, TS, Baum, E, Doubleday, N, Fiore, AM, Flanner, M, Fridlind, A, Garrett, TJ, Koch, D, Menon, S, Shindell, D, Stohl, A and **Warren, SG** 2008 Short-lived pollutants in the Arctic: their climate impact and possible mitigation strategies, *Atmos. Chem. Phys*, **8**: 1723–1735. DOI: https://doi.org/10.5194/acp-8-1723-2008

Roiger, A, Thomas, J-L, Schlager, H, Law, K, Kim, J, Schafler, A, Marelle, L, Raut, J-C, Weinzierl, B, Reiter, A, Rose, M, Dahlkotter, F, Minikin, A, Krisch, I, Scheibe, M, Stock, P, Baumann, R, Bouarar, I, Clerbeaux, C, George, M, Onishi, T and **Flemming, J** 2015 Quantifyng emerging local anthropogenic emissions in the Arctic region: the ACCESS aircraft campaign experiment, *Bull. Amer. Meteor. Soc*. DOI: https://doi.org/10.1175/BAMS-D-13-00169.1

Schaap, M, Roemer, M, Sauter, F, Boersen, G, Timmermans, R and **Builtjes, PJH** 2005 LOTOS-EUROS: Documentation, TNO report B&O-A, 2005–297, Apeldoorn.

Serreze, MC and **Barry, RC** 2011 Processes and impacts of Arctic amplification: a research synthesis, *Global Planet. Change*, **77**: 85–96. DOI: https://doi.org/10.1016/j.gloplacha.2011.03.004

Shindell, DT, Chin, M, Dentener, F, Doherty, RM, Faluvegi, G, Fiore, AM, Hess, P, Koch, DM, MacKenzie, IA, Sanderson, MG, Schultz, MG, Schulz, M, Stevenson, DS, Teich, H, Textor, C, Wild, O, Bergmann, DJ, Bey, I, Bian, H, Cuvelier, C, Duncan, BN, Folberth, G, Horowitz, LW, Jonson, J, Kaminski, JW, Marmer, E, Park, R, Pringle, KJ, Schroeder, S, Szopa, S, Takemura, T, Zeng, G, Keating, TJ and **Zuber, A** 2008 A multi-model assessment of pollution transport to the Arctic, *Atmos. Chem. Phys*, **8**: 5353–5372. DOI: https://doi.org/10.5194/acp-8-5353-2008

Stephenson, S, Smith, L and **Agnew, J** 2011 Divergent long-term trajectories of human access to the Arctic, *Nature Climate Change*, **1**: 156–160. DOI: https://doi.org/10.1038/nclimate1120.

Stockwell, WR, Kirchner, F, Kuhn, M and **Seefeld, S** 1997 A new mechanism for regional atmospheric chemistry modeling, *J. Geophys. Res*, **102**(D22): 25,847–25,879. DOI: https://doi.org/10.1029/97JD00849.

Stohl, A, Klimont, Z, Eckhardt, S, Kupiainen, K, Shevchenko, VP, Kopeikin, VM and **Novigatsky, AN** 2013 Black carbon in the Arctic: the underestimated role of gas flaring and residential combustion emissions, *Atmos. Chem. Phys*, **13**: 8833–8855. DOI: https://doi.org/10.5194/acp-13-8833-2013.

Tuccella, P, Curci, G, Visconti, G, Bessagnet, B, Menut, L and **Park, RJ** 2012 Modeling of gas and aerosol with WRF-Chem over Europe: Evaluation and sensitivity study, *J. Geophys. Res*, **117**(D03): 303. DOI: https://doi.org/10.1029/2011JD016302.

Vestreng, V 2003 Review and revision: Emission data reported to CLRTAP, EMEP/MSC-W Note 1/2003, 134 pp, *Norw. Meteorol. Inst, Oslo*. [Available at http://emep.int/publ/reports/2003/mscw_note_1_2003.pdf.]

Walcek, CJ and **Taylor, GR** 1986 A theoretical method for computing vertical distribution of acidity and sulfate production within clouds, *J. Atmos. Sci*, **43**: 339–355. DOI: https://doi.org/10.1175/1520-0469

Wesely, ML and **Hicks, BB** 2000 A review of the current status of knowledge on dry deposition, *Atmos. Environ*, **34**(12–14): 2261–2281. DOI: https://doi.org/10.1016/S1352-2310(99)00467-7

Wespes, C, Emmons, L, Edwards, DP, Hannigan, J, Hurtmans, D, Saunois, M, Coheur, P-F, Clerbaux, C, Coffey, MT, Batchelor, RL, Lindenmaier, R, Strong, K, Weinheimer, AJ, Nowak, JB, Ryerson, TB, Crounse, JD and **Wennberg, PO** 2012 Analysis of ozone and nitric acid in spring and summer Arctic pollution using aircraft, ground-based, satellite observations and MOZART-4 model: source attribution and partitioning, *Atmos. Chem. Phys*, **12**: 237–259. DOI: https://doi.org/10.5194/acp-12-237-2012

Wild, O, Zhu, X and **Prather, MJ** 2000 Fast-J: Accurate simulation of in- and below cloud photolysis in tropospheric chemical models, *J. Atmos. Chem*, **37**: 245–282. DOI: https://doi.org/10.1023/A:1006415919030

Wong, DN, Barth, M, Skamarock, W, Grell, G and **Worden, J** A Budget of the Summertime Ozone Anomaly Above Southern United States using WRF-Chem, AGU Fall Meeting, San Francisco, CA, USA, 14–18 December 2009.

Xiao, Y, Logan, JA, Jacob, DJ, Hudman, RC, Yantosca, R and **Blake, DR** 2008 Global budget of ethane and regional constraints on US sources, *J. Geophys. Res*, **113**(D21): 306. DOI: https://doi.org/10.1029/2007JD009415

Yang, Q, Bitz, CM and **Doherty, SJ** 2014 Offsetting effects of aerosols on Arctic and global climate in the late 20th century, *Atmos. Chem. Phys*, **14**: 3969–3975. DOI: https://doi.org/10.5194/acp-14-3969-2014

How to cite this article: Tuccella, P, Thomas, JL, Law, KS, Raut, J-C, Marelle, L, Roiger, A, Weinzierl, B, Denier van der Gon, HAC, Schlager, H and Onishi, T 2017 Air pollution impacts due to petroleum extraction in the Norwegian Sea during the ACCESS aircraft campaign. *Elem Sci Anth,* 5: 25, DOI: https://doi.org/10.1525/elementa.124

Domain Editor-in-Chief: Detlev Helmig, University of Colorado Boulder, US

Guest Editor: Brian Lamb, Washington State University, US

Knowledge Domain: Atmospheric Science

Part of an *Elementa* Special Feature: Oil and Natural Gas Development: Air Quality, Climate Science, and Policy

Submitted: 8 October 2016 **Accepted:** 21 April 2017 **Published:** 07 June 2017

ELEMENTA Science of the Anthropocene

Elem Sci Anth is a peer-reviewed open access journal published by University of California Press.

OPEN ACCESS